IR Spectral Signatures of the MILLRACE
Debris Cloud

R. P. GIGUERE, D. A. JONES, D. C. KAYSER,
C. J. RICE and R. W. RUSSELL
Space Sciences Laboratory
Laboratory Operations
The Aerospace Corporation
El Segundo, Calif. 90245

20 April 1983

DTIC
ELECTE
JUN 1 1983

A

Prepared for

SPACE DIVISION
AIR FORCE SYSTEMS COMMAND
Los Angeles Air Force Station
P.O. Box 92960, Worldway Postal Center
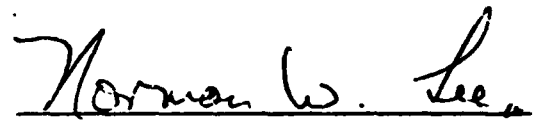Los Angeles, Calif. 90009

83 06 01 01

AD A128715

DTIC FILE COPY

This report was submitted by The Aerospace Corporation, El Segundo, CA 90245, under Contract No. F04701-81-C-0082 with the Space Division, Deputy for Technology, P.O. Box 92960, Worldway Postal Center, Los Angeles, CA 90009. It was reviewed and approved for The Aerospace Corporation by H. Rugge, Director, Space Sciences Laboratory . Lt Ken R. Hasegawa, SD/YLVS, was the project officer for the Mission-Oriented Investigation and Experimentation (MOIE) Program.

This report has been reviewed by the Public Affairs Office (PAS) and is releasable to the National Technical Information Service (NTIS). At NTIS, it will be available to the general public, including foreign nationals.

This technical report has been reviewed and is approved for publication. Publication of this report does not constitute Air Force approval of the report's findings or conclusions. It is published only for the exchange and stimulation of ideas.

Ken R. Hasegawa, 2nd Lt, USAF
Project Officer

Norman W. Lee, Jr., Colonel, USAF
Commander, Det 1, AFSTC

REPORT DOCUMENTATION PAGE	READ INSTRUCTIONS BEFORE COMPLETING FORM

1. REPORT NUMBER	2. GOVT ACCESSION NO.	3. RECIPIENT'S CATALOG NUMBER
SD-TR-83-29	*A12 8 715*	

4. TITLE (and Subtitle)	5. TYPE OF REPORT & PERIOD COVERED
IR SPECTRAL SIGNATURES OF THE MILLRACE DEBRIS CLOUD	
	6. PERFORMING ORG. REPORT NUMBER TR-0083(3940-03)-1

7. AUTHOR(s)	8. CONTRACT OR GRANT NUMBER(s)
R. P. Giguere, D. A. Jones, D. C. Kayser, C. J. Rice and R. W. Russell	F04701-82-C-0083

9. PERFORMING ORGANIZATION NAME AND ADDRESS	10. PROGRAM ELEMENT, PROJECT, TASK AREA & WORK UNIT NUMBERS
The Aerospace Corporation El Segundo, Calif. 90245	

11. CONTROLLING OFFICE NAME AND ADDRESS	12. REPORT DATE
Space Division	20 April 1983
Air Force Systems Command	13. NUMBER OF PAGES
Los Angeles, Calif. 90009	52

14. MONITORING AGENCY NAME & ADDRESS(if different from Controlling Office)	15. SECURITY CLASS. (of this report)
	Unclassified
	15a. DECLASSIFICATION/DOWNGRADING SCHEDULE

16. DISTRIBUTION STATEMENT (of this Report)

Approved for public release; distribution unlimited.

17. DISTRIBUTION STATEMENT (of the abstract entered in Block 20, if different from Report)

18. SUPPLEMENTARY NOTES

19. KEY WORDS (Continue on reverse side if necessary and identify by block number)

IR spectral signature   MILLRACE
Debris clouds   Solar radiation scattered by clouds
Dust clouds   Water clouds

20. ABSTRACT (Continue on reverse side if necessary and identify by block number)

Infrared radiation scattered by the dust and debris cloud generated by the detonation of 600 tons of Ammonium Nitrate/Fuel Oil (ANFO) high explosive for the MILLRACE test on 16 September 1981 was measured by an infrared spectrometer from a Learjet. The observations were made to characterize the signature of dust/dirt clouds and to compare such observations with similar measurements of naturally-occurring water clouds. The instrument used a circular variable interference filter in the spectral interval from 1.8 to

DD FORM 1473
(FACSIMILE)

19. KEY WORDS (Continued)

20. ABSTRACT (Continued)

3.4 µm to continuously scan solar radiation scattered by clouds. A total of 76 minutes of data was collected beginning with detonation. The cloud reached a stabilization altitude of 4.4 km MSL (2.9 km AGL). The Learjet's flight plan was structured to permit characterizing the scattered radiation as a function of wavelength, scattering angle, and time from detonation. Scattering angles from about 50 to 180 deg were sampled. The expected increase in scattered flux at smaller scattering angles was observed; the wavelength dependence of this effect has not yet been fully determined. Cumulus clouds present in the area were also observed. When compared with measurements and calculations for water clouds, the radiation scattered from the dust cloud exhibits higher relative intensity in the wavelength region beyond 3.0 µm. Specifically, the ratio of the intensity of scattered radiation at 3.1 to 3.3 µm to that at 2 µm is 5 to 10 times larger for thick dust clouds than for water clouds.

Accession For

NTIS GRA&I

DTIC TAB

Unannounced

Justification

Availability Codes

TABLE OF CONTENTS

Figures

I. INTRODUCTION

The MILLRACE[1] high explosive test sponsored by the Defense Nuclear Agency (DNA) involved the detonation of 600 tons of an ammonium nitrate-fuel oil (ANFO) mixture in order to simulate the environmental effects of the air-blast and shock which would result from exploding nuclear weapons. Detonation occurred at 12:35:39 MDT on 16 September 1981. The surface explosion also generated a large cohesive cloud of dust, dirt and debris which rose from the detonation site to an altitude of about 4.4 km mean sea level (MSL), (2.9 km above ground level, AGL), and was then carried away from the blast site by the prevailing winds. The test thus represented an excellent opportunity to obtain measurements of the infrared signature of heavily dirt-laden clouds. The experiment described here measured the infrared radiance from the debris cloud as a function of wavelength, angular position relative to the sun, and time from detonation. These measurements could then be compared with similar measurements and theoretical calculations for typical water clouds.

In the IR band between 1.8 and 3.4 μm, a dirt cloud is seen by scattered solar radiation, not by self-emission as would be the case, for example, near 10 μm. The background signal from other sources in the field of view must also be considered. The angular relationships are shown in Figure 1. Note in particular that the scattering angle is defined as the angle of deviation from the original ray path, e.g., radiation scattered directly back to the source has a scattering angle of 180 deg. In general, scattering functions are highly peaked in the forward direction (near 0 deg), a phenomenon familiar to everyone who has seen the brilliant outlining of the edges of a small cloud which has moved in front of the sun.
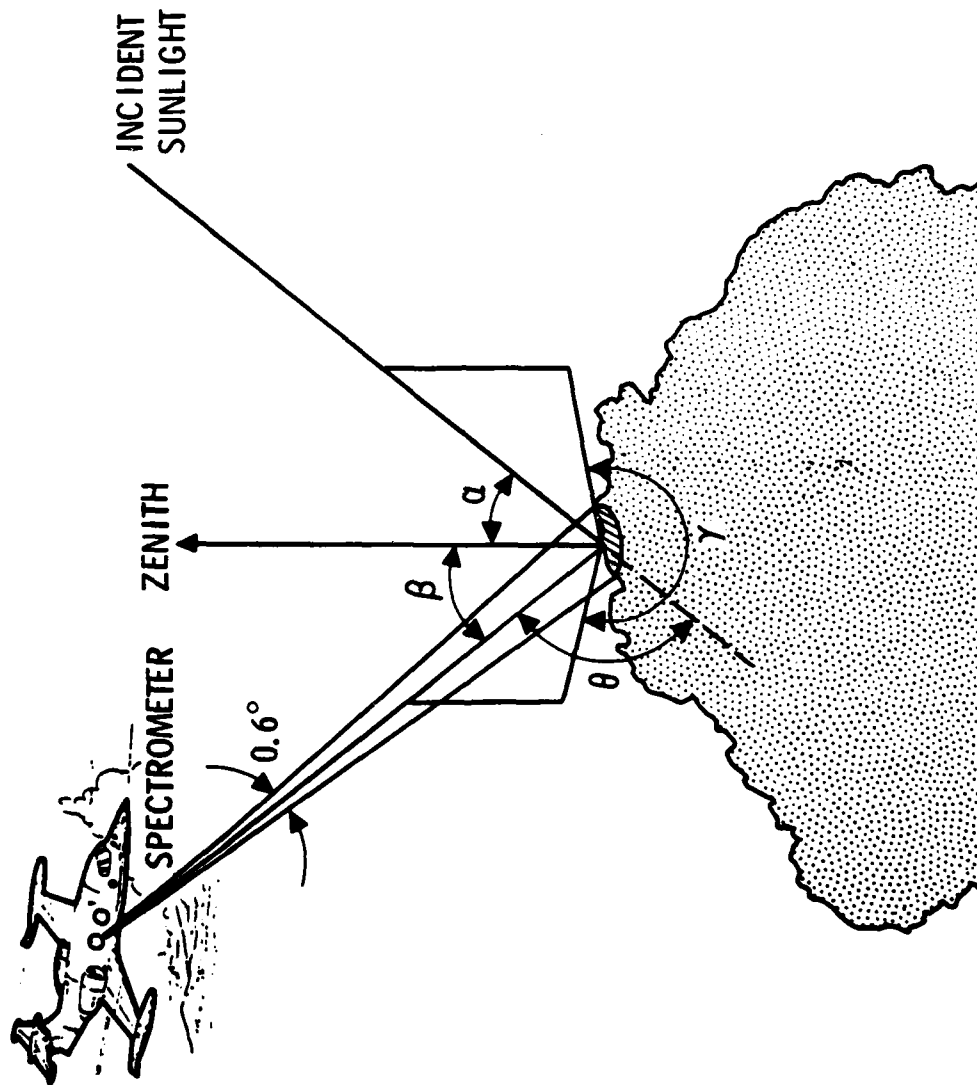
Figure 1. Sun-Cloud-Aircraft Geometry α = Solar Zenith Angle, β = Sensor Zenith Angle, γ = Azimuthal Difference, and θ = Scattering Angle

4

II. EXPERIMENT DESCRIPTION

A. INSTRUMENT DESCRIPTION

The DEMON instrument is a small, hand-guided infrared spectrometer designed for operation on a Learjet aircraft. A somewhat schematic representation of the infrared spectrometer is shown in Figure 2. For the MILLRACE test the instrument employed a circular variable interference filter (CVF) to scan the infrared radiation scattered from the debris cloud in the wavelength interval 1.8 to 3.4 μm. Prior to the MILLRACE Test the DEMON instrument had been configured as a 6-detector filter radiometer operating in three nonoverlapping spectral bands. In this form the detectors could be optimized for the expected intensities in each wavelength band though at the sacrifice of detailed spectral information. For MILLRACE we chose to concentrate on spectral information and hence configured the instrument as an infrared spectrometer.

As a spectrometer, the DEMON instrument utilizes a circular variable interference filter to scan the region between 1.77 and 3.42 μm. A CVF consists of an interference filter deposited on a circular substrate. The wavelength transmitted by the CVF varies linearly with angle around the circumference of the filter so that as the filter spins in the optical beam the transmitted wavelength scans from one end of the passband to the other and then back again. The percentage bandwidth of the filter is relatively constant at all wavelengths. The DEMON CVF has an intrinsic resolution $\lambda / \Delta \lambda$ of 60. The optical beam traversing the filter is somewhat larger than optimum, however, resulting in a slightly degraded resolution of 40 to 50. The CVF is spun at 1.2 rad/sec giving a complete double-scan spectrum in 5.2 sec. Ribs used to strengthen the filter housing periodically block the beam and thus can act as excellent fiducial marks as well as providing opportunities to determine the noise level and zero signal
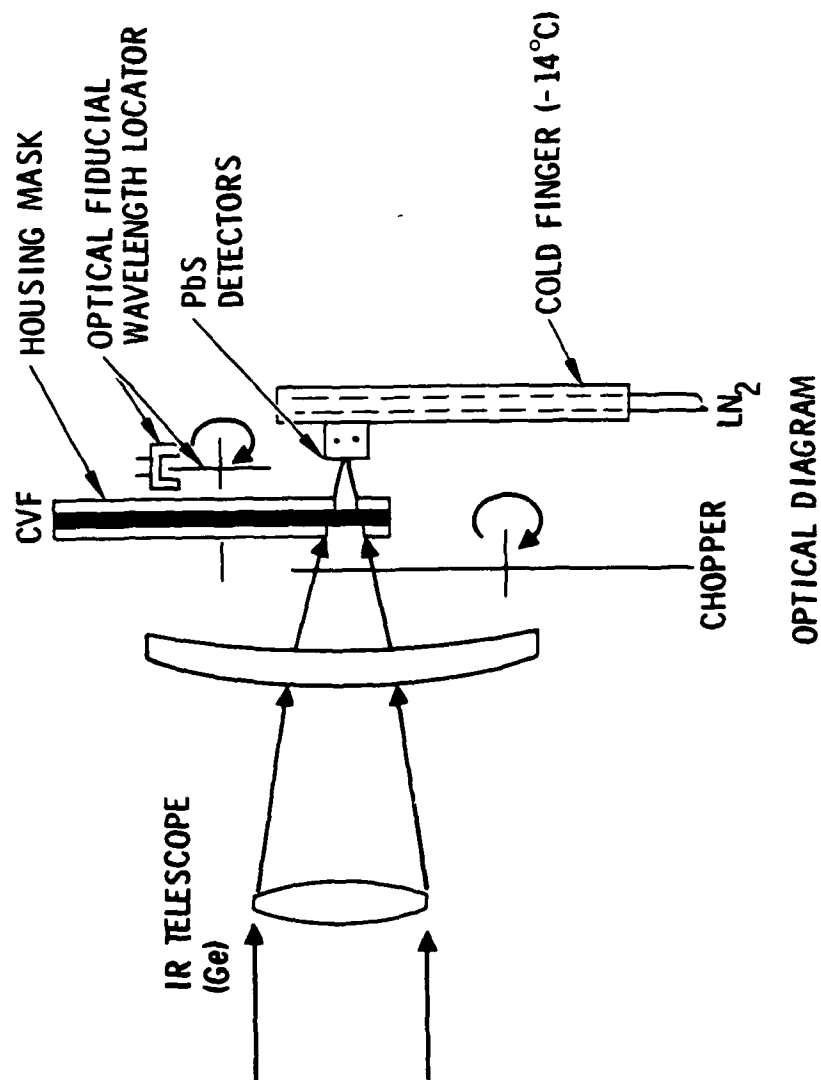
5

HOUSING MASK

OPTICAL FIDUCIAL
WAVELENGTH LOCATOR

PbS
DETECTORS

COLD FINGER (-14°C)

CVF

LN$_2$

CHOPPER

OPTICAL DIAGRAM

IR TELESCOPE
(Ge)

Figure 2. Optical Diagram of the Infrared Spectrometer

6

level of the detectors. The ribs are placed at either end of the spectrum and in the CO_2 absorption band where no usable signal would be expected in any case.

Two ambient temperature PbS detectors manufactured by Santa Barbara Research Center are mounted on the focal plane. The detectors are ~1 mm square and have response curves peaked near 2.6 μm. The detectors are cooled by circulating LN_2 and cold N_2 gas through cooling tubes in the mounting block; the temperature is monitored by thermocouples. The inst   ent housing is also purged with the cold dry nitrogen gas in order to stal   'ze the tem-perature of the chopper wheel, avoid condensing water on tr   :ooled com-ponents, and minimize water in the optical path. Though non   -   .y ambient temperature devices, we found the best operating temperature for this pair of PbS detectors to be -14°C. This temperature optimizes both detectors for the largest signal and thus, because we are not detector-noise or background-limited, for the highest signal to noise ratio (SNR). The optical signal is modulated at 500 Hz by a chopper wheel inside the instrument in order to have a reference for synchronous detection. The amplifier time constant is 5 msec. The gains of the two detectors are set electronically to differ by a factor of 4, resulting in an overall dynamic range of 400. The detectors view slightly different portions of the scene; the relative position of each is indicated in the view finder so that the experimenter sighting the instrument can guide the feature of interest onto either of the detectors or alternate between them.

The instrument uses a single f/1.5 doublet lens. The 6.95-cm di-ameter lens is made of germanium; the focal length is 10 cm. The effective diameter of the lens as mounted is 6.05 cm. The lens has an antireflection coating which yields ~90 percent transmission across the band of interest except near the short-wavelength cutoff at ~1.8 μm. The focal plane of the lens was determined in the laboratory with a laser at 3 μm.

7

The entire instrument is mounted inside the cabin of the Learjet in what is essentially a normal laboratory environment. A schematic drawing of the cabin installation is shown in Figure 3. A special-purpose window mounting with two ports located side-by-side replaces an emergency escape hatch on the right side of the aircraft. The aft port is used by the DEMON instrument itself and consists of two 8-in. diameter 0.25-in. thick sapphire windows mounted in a double-pane configuration. An 8-mm movie camera views through the left (forward) port which utilizes plexiglass windows, also in a double-pane mounting. The double-pane mount is required because of heavy frosting frequently encountered when operating at high altitude. Additionally, electrical heating tape is wrapped around the periphery of the assembly.

The instrument and the 8-mm movie camera are slaved together on a two-axis gimballing platform so that both instruments always look in precisely the same direction. The movie camera provides both a view finder for spotting the spectrometer at specific cloud features and a running visible-light record of the scene at 1-sec intervals. A block of light-emitting diode digits is imaged on the upper edge of the film to provide time and date. A hand-held 35-mm camera was used to take color photographs of the general scene; these photographs were also time-tagged.

Nitrogen gas for cooling the focal plane and purging the instrument is obtained from the boil-off gas from a 25-liter liquid nitrogen dewar. This dewar is mounted in a restraining frame just below the instrument. A rack containing electronics is mounted just forward of the nitrogen dewar. A panel in this rack provided the capability to control and monitor the instrument. Two redundant cassette tape recorders record the output from the two detectors, the time code generator, the aircraft autopilot, instrument
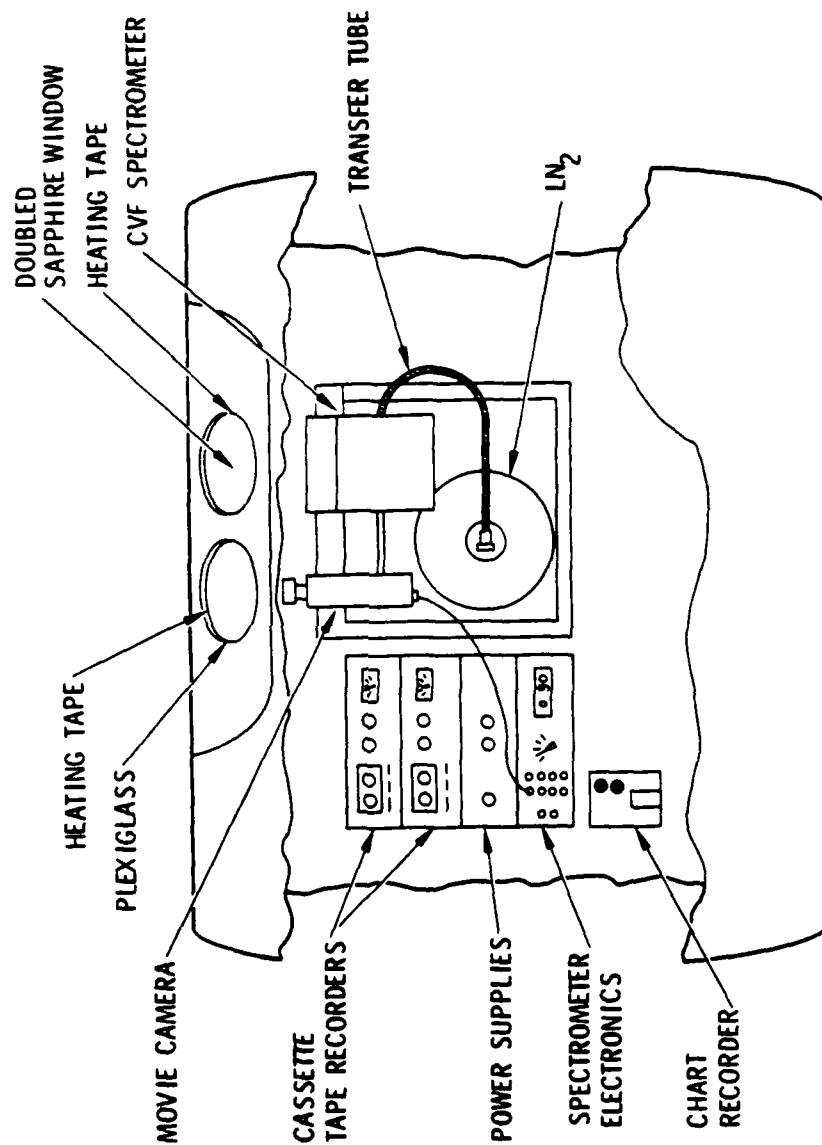
8

DOUBLED
SAPPHIRE WINDOW

HEATING TAPE

CVF SPECTROMETER

TRANSFER TUBE

LN$_2$

HEATING TAPE

PLEXIGLASS

MOVIE CAMERA

CASSETTE
TAPE RECORDERS

POWER SUPPLIES

SPECTROMETER
ELECTRONICS

CHART
RECORDER

Figure 3. IR Observation System – Learjet Installation

9

gimbal-axis position indicators, and various housekeeping monitors. In addition, the data are fed to a Brush recorder so that signals can be monitored in real time.

B.   CALIBRATION

Measurement of the responsivity of each detector as a function of wavelength is of primary importance in measuring absolute radiances. Calibrations are generally performed end-to-end, i.e., all elements normally in the beam in flight are present during calibration. The exception is the aircraft window; window transmission over the entire band is extremely flat, however, with a measured value of 76 percent.

Calibration of the instrument consisted of measurements of wavelength versus the CVF rotation angle and of the field-of-view, alignment, and responsivity as a function of wavelength and detector temperature. The primary infrared radiation source employed for the calibration was a Barnes Model 11-200 blackbody source which operates at any selected temperature in the range 200 to 1000°C. The absolute flux calibration was made with an NBS secondary standard blackbody made by IR Industries.

The angular response for each detector is approximately square and for both elevation and azimuth is ~0.6 deg FWHM. Small asymmetries appear as a result of known aberrations in the lens system. For this flight the area of interest is typically greater than the field-of-view so that such features are not really significant. Generally we ignore times when the character of the scene is changing rapidly (as a result of scanning over cloud margins, for example).

C.   DATA REDUCTION

The data reduction process used to obtain spectral signatures of natural and artificial clouds is outlined in Figure 4. Obtaining the spectral signature of a cloud requires more than just processing the
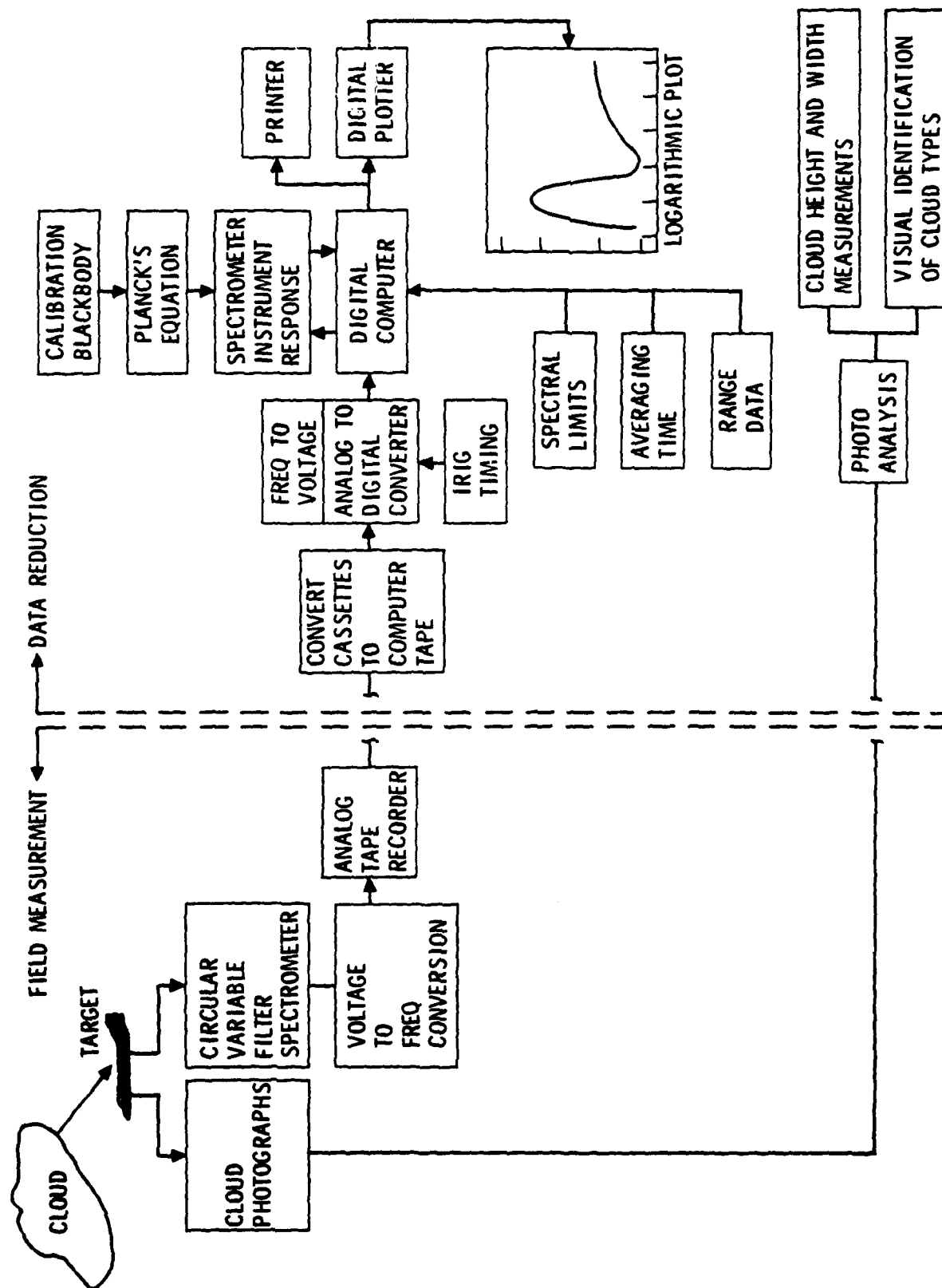
10

Figure 4. Data Reduction Procedure

11

spectrometer data for the IR spectra. In order to determine the scattering angle it is necessary to know the elevation and azimuth position of the sun and the aircraft and of the spectrometer relative to the aircraft, and also the height of the cloud and its distance. The aircraft coordinates are obtained from the ground radar track. The sun's elevation and azimuth angles are readily calculated from the time of day as shown in Figure 5. The elevation and azimuth positions of the spectrometer are obtained from the two-axis gimballing platform and are recorded with the IR data on the tape recorders. The cloud height and width are estimated from photoanalysis of the ground-based movie films and our own Learjet observations.

The processing of the spectrometer's IR data can be best understood by explaining how the spectrometer records the data in the field. As the spectrometer scans a target, the zero signal level for each detector is also recorded. This internal reference is provided by the four support ribs of the filter housing which briefly block the detectors during each scan. The ribs are positioned on the wheel to coincide with the beginning and end of the filter passband and in the atmospheric transmission minimum between 2.6 and 2.75 μm. The signal from each detector is synchronously detected and amplified by its own lock-in amplifier. Such a technique is required to maximize the signal-to-noise ratio during amplification of the low-level signals. Next, the signals from each detector are FM modulated in a voltage to frequency conversion and redundantly recorded. Each detector has a separate frequency channel. Additional data such as the focal plane temperature, elevation and azimuth of the spectrometer, the time, and the CVF fiducial mark are also FM encoded on separate FM channels and recorded along with the spectrometer data on both tape recorders. The clock signal also triggers the 8-mm movie camera at 1-sec intervals. The 35-mm camera is independently operated by hand. During the field measurements, the crew also
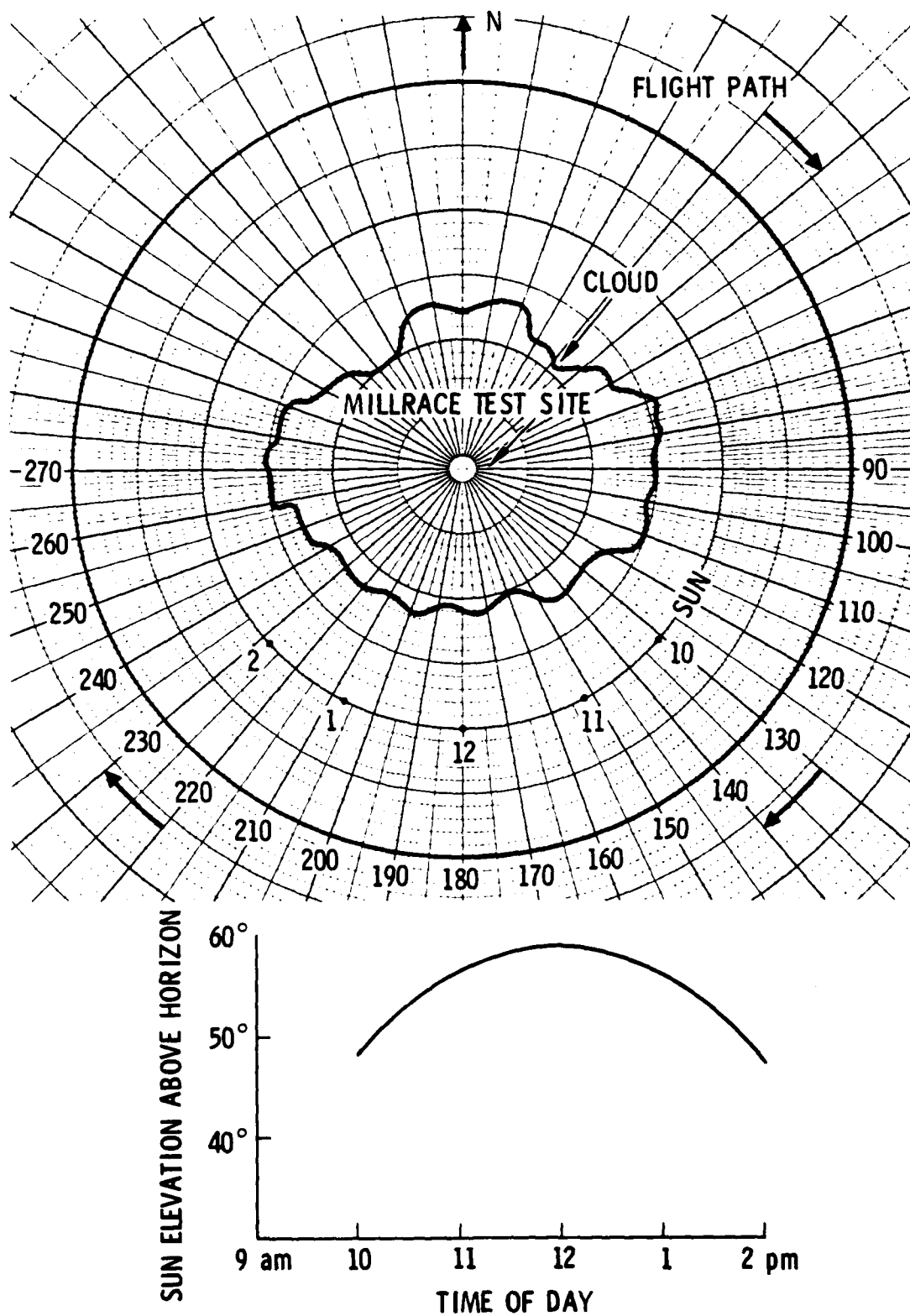
12

Figure 5. Solar Azimuth and Elevation Angles versus Time of Day: 16 September 1981

monitors a chart recorder which displays the amplified detector signals and the angular position of the filter wheel, i.e., the raw IR spectra. The crew base their selection of the appropriate optical attenuation for the spectrometer on these raw IR spectra.

After the field measurements, the data on the cassette tapes and an external IRIG time code are transcribed onto a computer-compatible tape; the data channels are decoded by FM discriminators and then digitized at 200 samples/sec into computer tapes. The 200 samples/sec digitizing rate is selected to match the 5-msec sampling rate (time constant) of the lock-in amplifier and to obtain the maximum real information available from the tape. The data channels are unpacked from the tape and a correspondence between the CVF angular position (equivalent to wavelength) and the detector output is established for all the data of the mission. The IR spectra are still in the form of raw voltage levels. To convert this voltage to flux, a $300^{\circ}C$ blackbody calibration source was used in the laboratory to derive the instrument response. Using Planck's equation to determine the flux and correcting for the atmospheric attenuation of the laboratory air between the blackbody and instrument, the spectral response for this spectrometer was derived as shown in Figure 6. Compensation for nonlinear response of the electronics is achieved by comparing any nonlinear output voltage to the expected linear voltage as the blackbody flux is increased.

During the data processing the IR data are filtered digitally by averaging eight consecutive sampling points. This averaging reduces the data to a maximum bandwidth of 25 Hz. This decrease in data bandwidth does not significantly affect the instrument resolving power as it still allows two samples per CVF resolution element but does greatly reduce the overall noise background. A digital plotter produces the final spectral plots. The IR
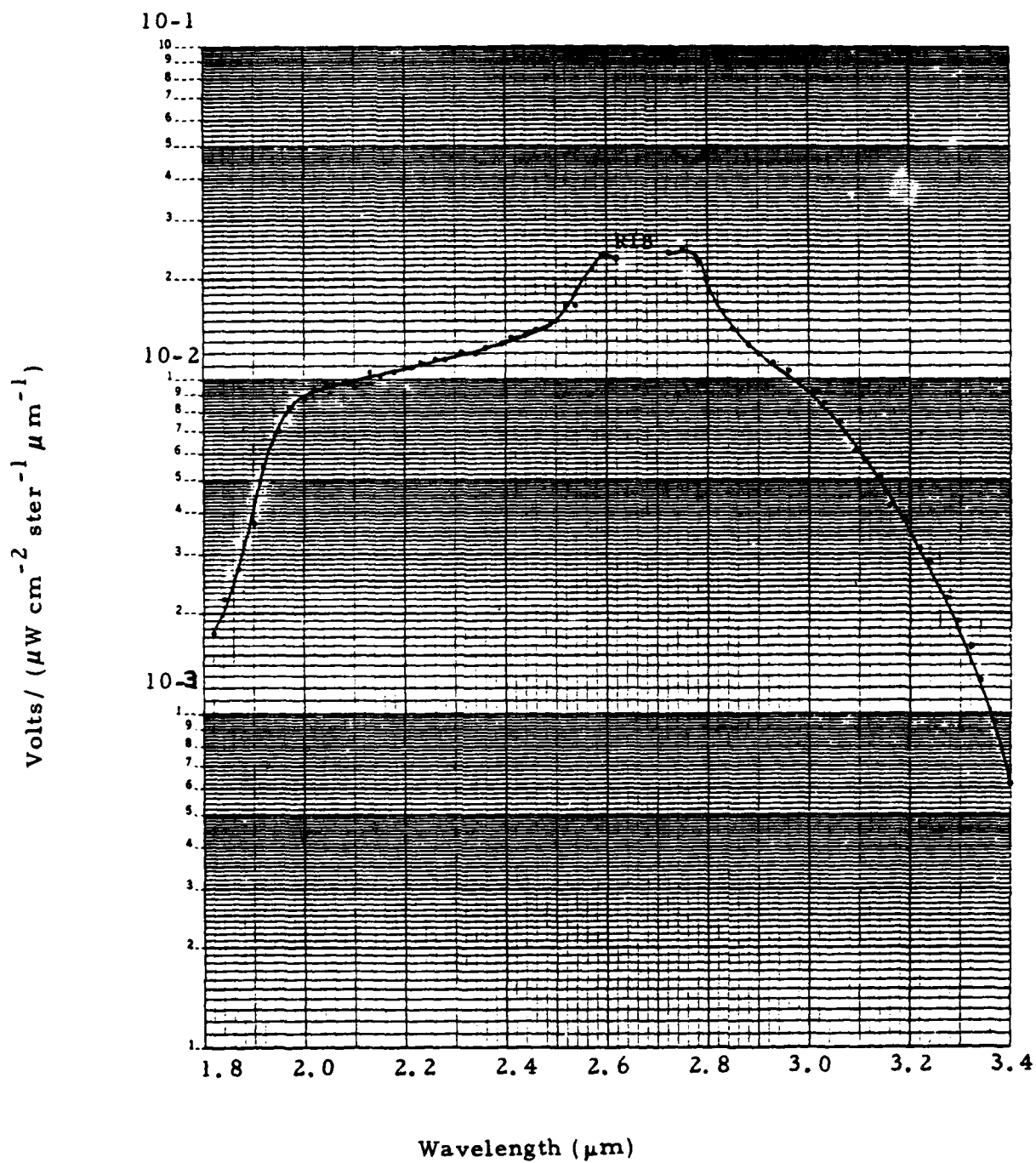
14

Figure 6.   Typical Spectral Response of IR Spectrometer – Detector D3

spectra, focal plane temperature, time, and elevation and azimuth position of the spectrometer are also printed.

The computer program incorporates the option of averaging successive spectra coherently. Coherent averaging improves the signal-to-noise ratio of the plotted spectra by the square root of the number of averaged spectra. This feature is particularly important for backgrounds in which intensity levels are low and the observation parameter does not change greatly between successive scans. Up to 42 seconds of data (eight double spectra) have been averaged to obtain some of the data presented in this report.

III. FLIGHT OBSERVATIONS

A. CLOUD MOTION

The MILLRACE explosive charge consisted of 600 tons of ANFO explosive material packed in individual 50-lb paper sacks which were then stacked on a wooden base in a beehive shape 9.1 m in diameter by 11.4 m in height. The detonation of the ANFO explosive (approximately equivalent to a 1 kt nuclear blast) produced a large, heavily dirt-laden cloud which stabilized by about T+6m at an altitude of ~4.4 km MSL (approximately 2.9 km above the desert floor). At the time of stabilization the cloud was approximately 2.5 km in diameter and extended over an altitude range of 1 1/2 to 2 km (ignoring the stem). The total mass of dirt lofted was perhaps 4 to 10 kt, based on the similarly-sized DICE THROW[3] high explosive test which took place some 8 km to the northwest. The soil at the site is a mixture of primarily fine-grained sand and silt to a depth of $3.4\,\mu$m with some coarser-grained sand at greater depth. Because it had rained the previous day it is probable that the debris cloud contained a higher proportion of water than would normally be the case for a detonation at White Sands. The presence of water clouds at the stabilization altitude also points to

16

somewhat greater atmospheric water content than might normally be expected at this high-desert location.

Figures 7 and 8 show the vertical rise of the peak and horizontal expansion of the debris cloud as a function of time. The values were determined by scaling from films kindly lent to us by John Cockayne of Science Applications Inc. and must be considered preliminary. The films used were made at two sites, Atom and Granjean. The distance and azimuth to these sites from ground zero are given in Table 1. The view directions are almost perpendicular to one another yielding a good picture of the overall cloud development. It was necessary to pan the camera to keep the cloud in the field of view. Normally the elevation and azimuth of the camera are indicated by a coded matrix at the bottom of each frame. We only had available to us 16-mm copies of the 35-mm originals; the copy process had deleted part of the coding matrix with the result that we can only follow the altitude development for a limited period, viz., 2 min for the Atom site and 7 min for the Granjean site. As can be seen in Figure 7, the debris cloud had essentially reached the stabilization altitude by T+7 min. Figure 7 shows the altitude of the cloud top as determined by visual sighting and the aircraft altimeter. This value, 4.4 km MSL (2.9 km AGL), is somewhat below the maximum determined photographically from the ground. Because we believe the altimeter readings to be essentially correct, it is possible that some rebounding may have occurred after T+7 min or that there may be some errors in the photographic determinations. (Note that there have been first-order corrections to our cloud height estimates for geometric effects arising from wind-driven motion of the cloud. The wind velocity versus altitude readings, as shown in Figure 9 were part of the ground observations made by Jack Reed of Sandia[5].)
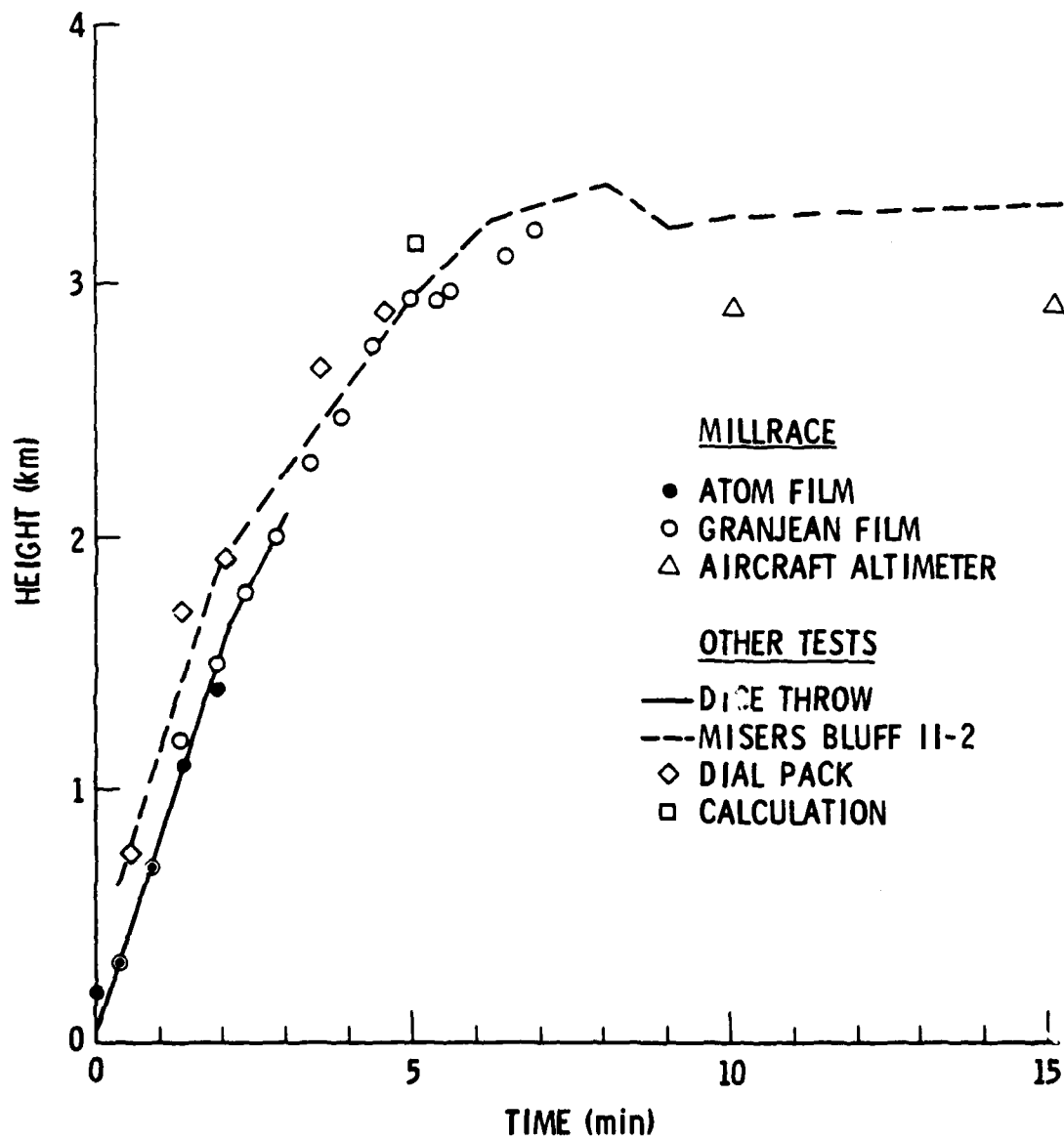
17

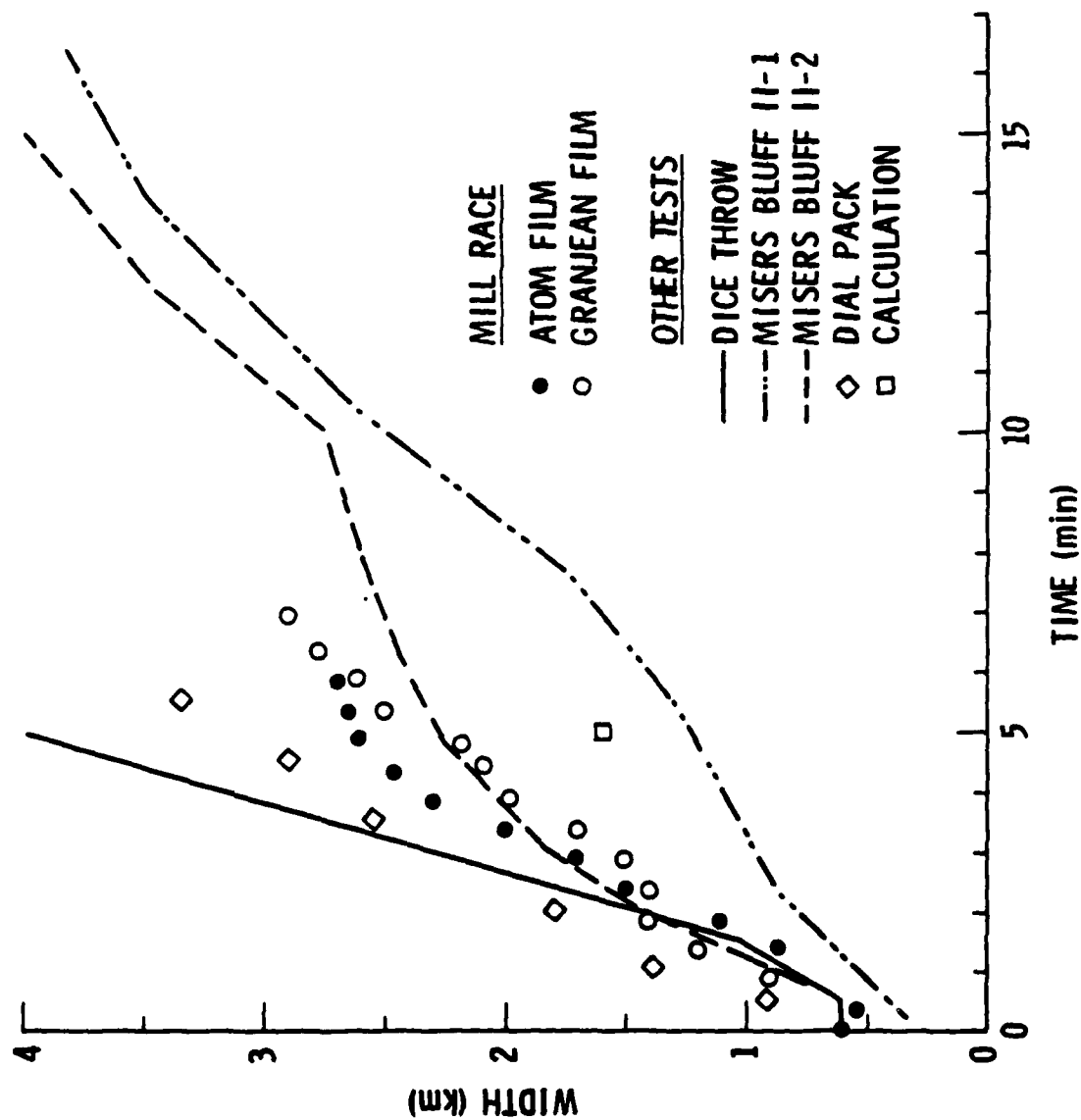Figure 7. Vertical Rise of Debris Cloud Peak versus Time

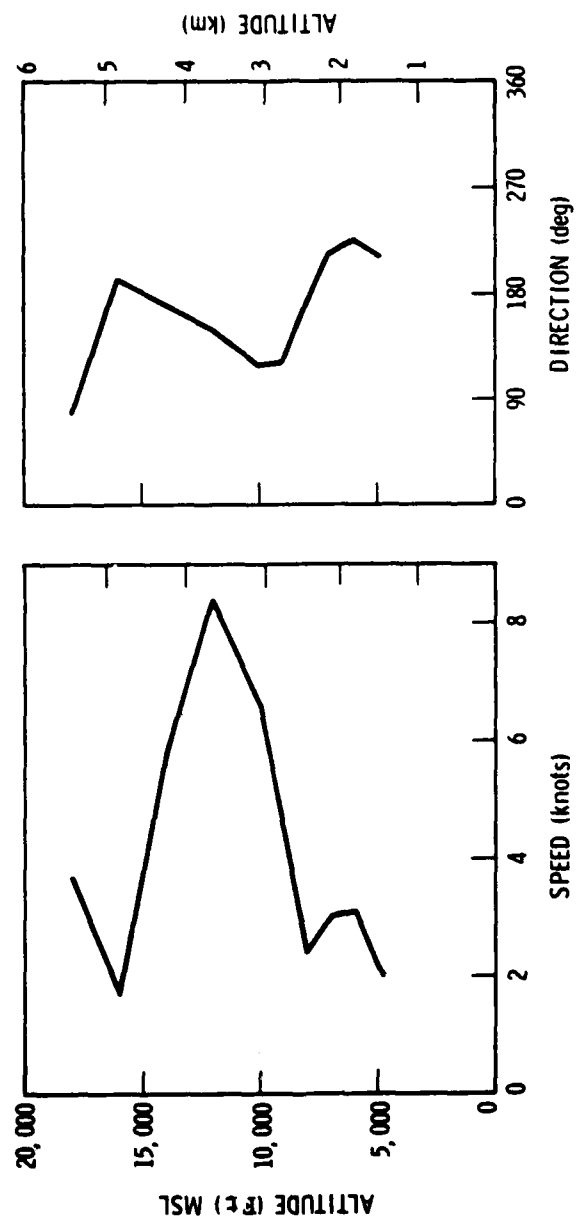Figure 8. Horizontal Expansion of the Debris Cloud versus Time

Figure 9. Wind Velocity versus Altitude

Table 1. Photographic Sites Used for Cloud Parameter Determination

Site	Azimuthal from Ground Zero (deg)	Distance (km)
Atom	37	17.2
Granjean	291	19.2

According to Ref. 4, the debris cloud created by a large explosion will rise buoyantly for about 2 min, after which turbulent expansion will continue until the cloud reaches stabilization. The turbulent expansion may give the appearance of continued buoyant rise. Internal motion after stabilization is driven by diffusion and wind shear. The height-time profile in Figure 7 does in fact show a break in the slope near 2 min. The cloud rose at about 12 m/s for the first 2 min (up to 1.6 km AGL) and then at about 7 m/s for the next 3 min (up to 3 km AGL). Nevertheless, the center of the expanding cloud rose 1.2 km between T+2 and 5 min (from 1.0 to 2.2 km AGL), indicating that the major part of the rise was still driven by buoyancy. At stabilization the cloud was about 1.5 km from top to bottom.

B.   FLIGHT OPERATIONS

The flight plan was structured to permit characterizing the scattered radiation as a function of wavelength, scattering angle and time from detonation. We recorded the IR signatures for 76 min beginning with detonation and ending at a time when wind shear and diffusion had produced a dispersed cloud. The water clouds present throughout the flight enabled side by side comparison of natural and artificial clouds under similar environmental conditions. The major details of our flight observations and maneuvers follow.

The Learjet left the Alamogordo airport at 1200 MDT in preparation for the MILLRACE test then scheduled for 1230 MDT. The aircraft flew north to a designated holding area some 20 km north of the actual detonation site.

21

Safety requirements dictated that the Learjet not be present in the area over ground zero at detonation because of other activity in the airspace, primarily a light plane taking photographs and 4 instrumented canisters which were parachuted from 10.6 km MSL during the 90 sec prior to detonation. The Learjet was therefore to remain in the holding area about 20 km north until the other airplane and the canisters, which were being tracked by radar, were out of the controlled airspace.

At T-3 min we positioned our plane in a straight run west to east with the starboard observation and IR instrumentation ports facing toward the test site. At T=0 we were about midway in our traverse and at the minimum distance of 18 km from ground zero. Our motorized 35-mm camera and IR instrumentation recorded the first minutes of the development of the debris cloud (Figures 10a-f). We experienced a very mild, short turbulence as the detonation shock wave passed; the pilots also observed a very rapidly expanding hemispherical rainbow (prism) effect produced by the shock-induced localized change in the air density and hence in the index of refraction. For the following 13 min we continued our observations from a distance.

At T+10 min, we were vectored into the cloud region by range control. We began by circling the debris cloud at 14,000' MSL (4.2 km) in a right banking turn with a 4.5 km radius. The altitude of the top of the debris cloud was observed to be at ~4.4 km MSL (2.9 km AGL). This was slightly lower than expected based on nuclear cloud models and the similarly-sized Misers Bluff II-2 test[7] (see earlier discussion on cloud heights). After making a complete circle of the cloud we began a series of maneuvers designed to maximize and systematize the angular coverage while emphasizing ranges of angles of particular interest. The most significant of these maneuvers are shown in Figures 11a-d. The aircraft never penetrated the debris cloud, nor, indeed, came closer than about 1 km, but only circled around the outside.
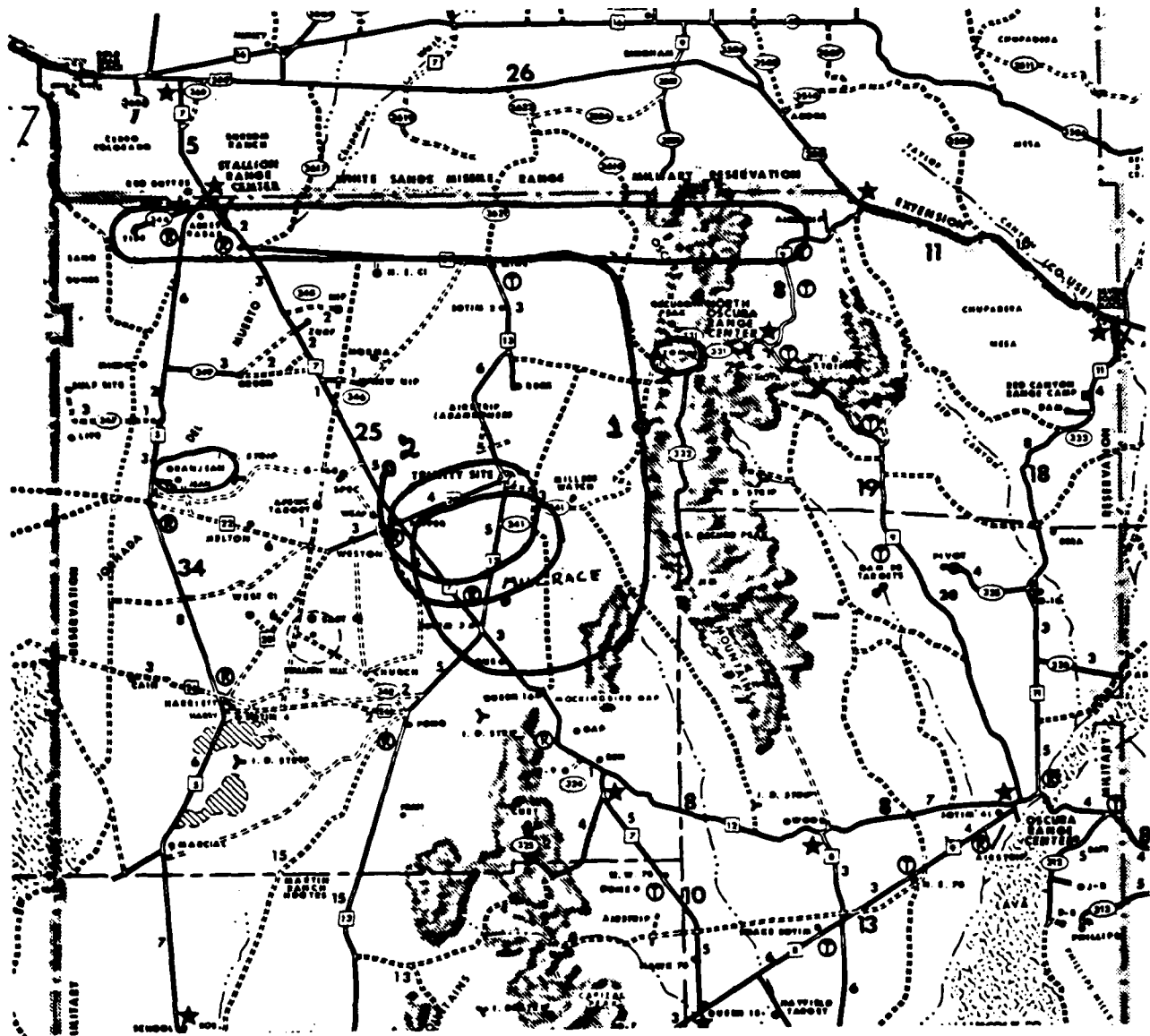
22

T + 1 sec

T + 2 sec
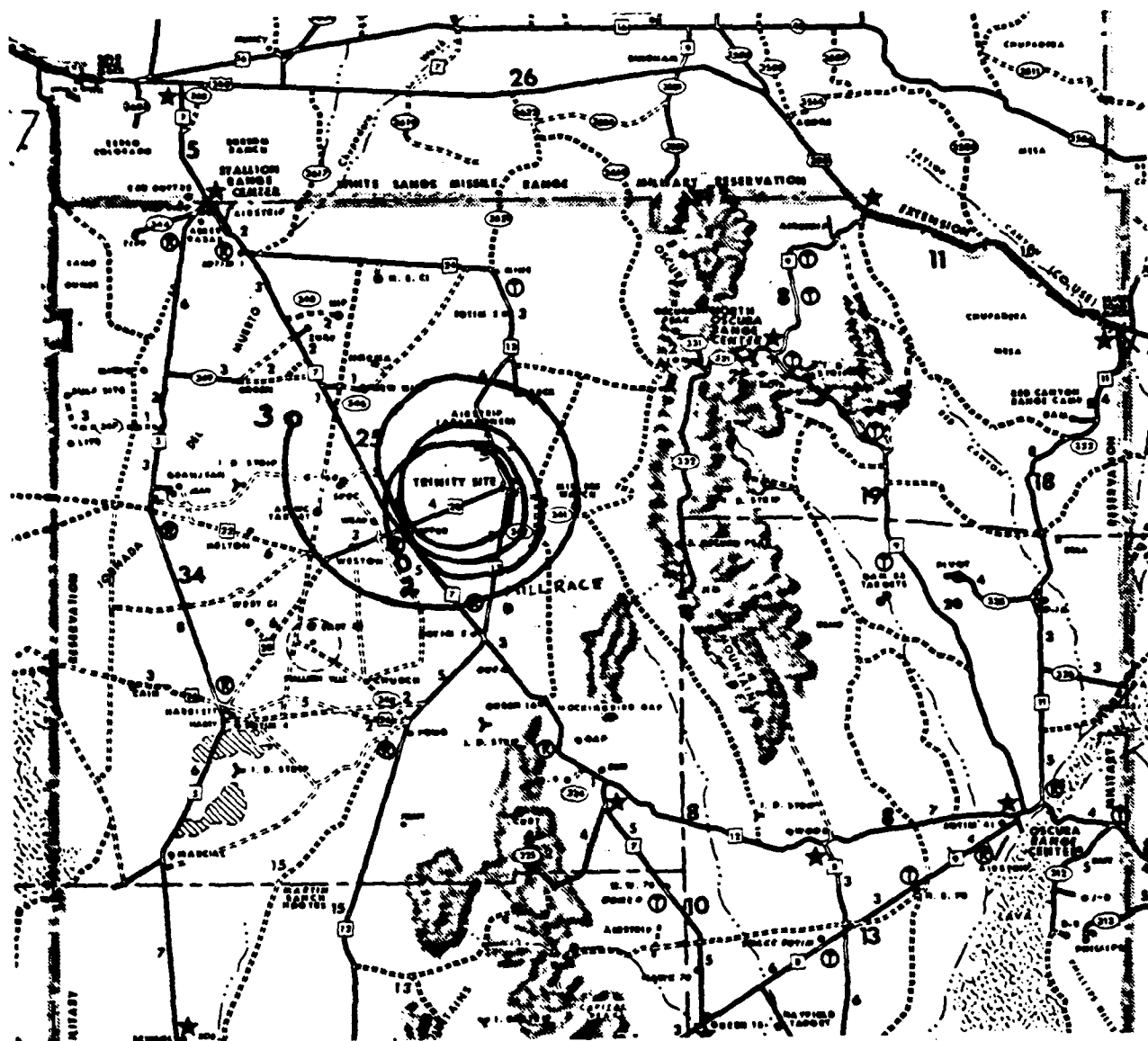
T + 3 sec

T + 14 sec

T + 38 sec

T + 85 sec

Figure 10a-f.   Photographs of the First Few Seconds of the Explosion as
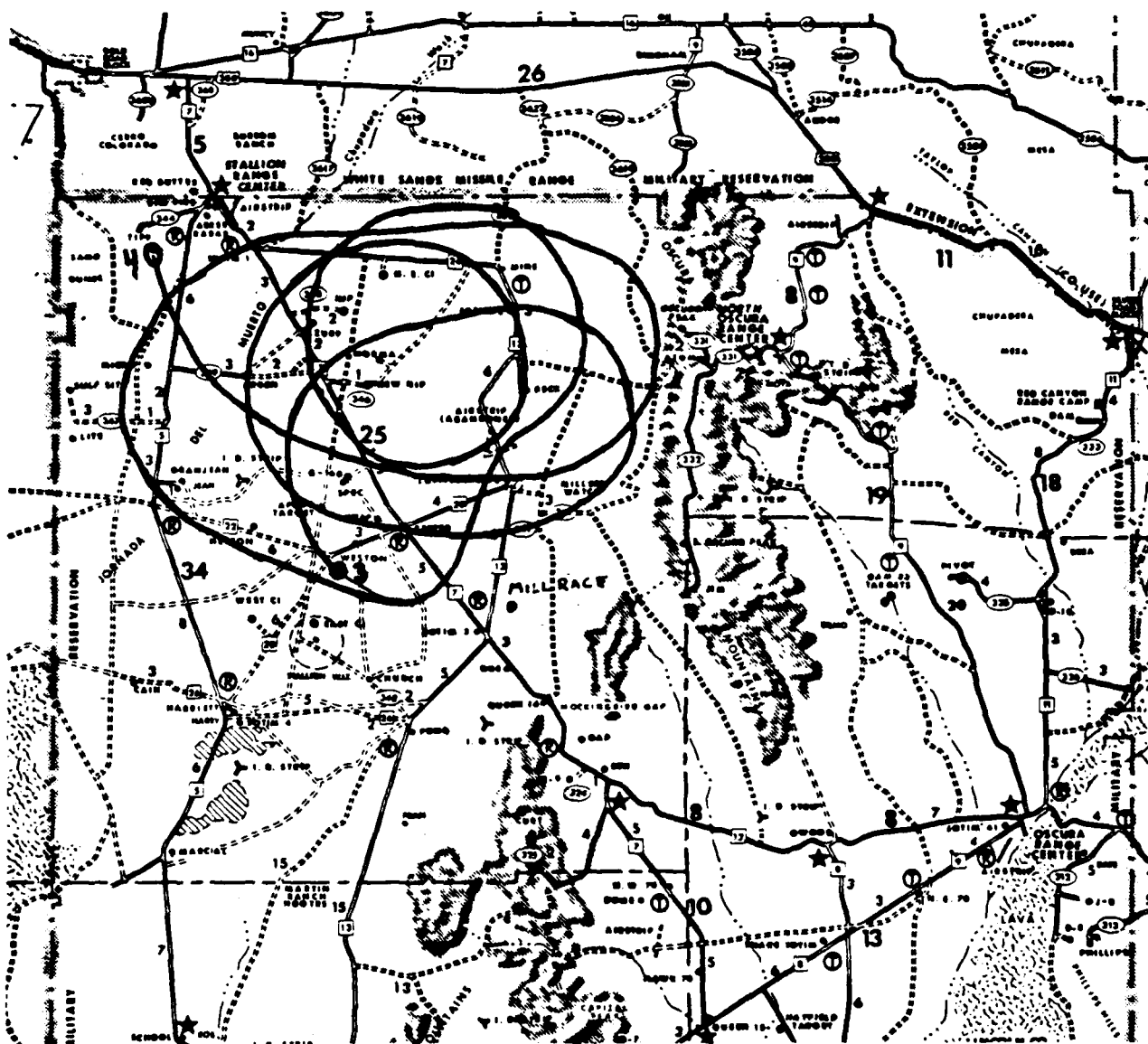Seen by the Learjet

23

GENERAL ROAD MAP - RANGE AREA

Figure 11a.   Flight Path of Aircraft

24

SCALE IN MILES

SCALE 1"=30,000 FT.

GENERAL ROAD MAP-RANGE AREA

Figure 11b. Flight Path of Aircraft

SCALE IN MILES

SCALE 1" = 30,000 FT.

GENERAL ROAD MAP - RANGE AREA

Figure 11c.   Flight Path of Aircraft

SCALE IN MILES

SCALE 1"=30,000 FT.

GENERAL ROAD MAP - RANGE AREA
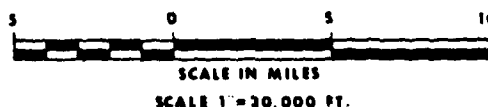
Figure 11d. Flight Path of Aircraft

With the sun to the rear, we first banked right into a straight line heading of 18 deg at a distance of ~1 km from the cloud edge (Figure 11a), the entire revolution around the cloud forming a "D"-shaped ground track. A second revolution was executed in a similar manner with the circular path on sunlight side.

At T+20 minutes we rose to 5.5 km MSL altitude (~1.1 km above the cloud top) and resumed right banking turns around the cloud for a series of four different bank angles (Figure 11b). The first revolution was with a 40 deg bank in a 2-mile turn radius; the second with a 35 deg bank and 2-mile radius; the third with a 25 deg bank and 2 1/2 mile radius; and the fourth with a 15 deg bank and 4-mile radius. These maneuvers were designed to determine the IR signature variation over a wide range of observation angles with respect to the sun.

At T+35 minutes, we returned to 4.5 km altitude, essentially level with the cloud top, and concentrated on scanning over the diffuse edges of the cloud. When possible we would scan onto nearby water clouds. The aircraft executed a continually growing spiral, Figure 11c, in order to permit integrated observations to be made over larger areas of the cloud. The spiral eventually reached a radius of about 8 km.

By the time this sequence, Figure 11d, was completed at T+66 min the debris cloud had become relatively diffuse, particularly at its periphery, but was still visually opaque elsewhere. In order to permit observations at low scattering angles we flew at 3.6 km altitude with the right side of the plane banked upward 45 deg toward the sun. Scattering angles as low as perhaps 20 deg were achieved. Because the edge of the cloud was somewhat diffuse, however, the scattering conditions may not be directly comparable with readings taken much earlier in the flight. The data gathering was broken off at T+76 min by which time the dispersing cloud had begun to merge visually with the background of water clouds.

C.   EXPLOSION GENERATED WATER CLOUD

Ground photography shows that the debris cloud had developed a cap of condensed water perhaps as early as T+3.5 min. By that time the cloud top had reached a height of ~2.2 km above ground (see Figure 12). Although this water cap was not so readily identifiable from our observing platform in the air, this ground observation is consistent with radiosonde data (Jack Reed, private communication[5]) which indicate that a rise of about 5000 ft (1.5 km) would bring the temperature of the rising air mass to the local dew point. At T+9.5 min we observed from the Learjet what appeared to be a small convective water cloud rising from the top of the debris cloud. The latter had essentially stabilized by this time. The small cloud appeared to be completely water, not a water-capped dirt plume, but it is not identifiable in the ground photography. This cloud dissipated after several minutes. The cloud (or, more properly, the plume) is intriguing because of the possibility that it implies an essentially dirt-free convective column within the overall cloud. Green[6] reported that a dust-sampling aircraft which penetrated the debris cloud produced by DIAL PACK at T+9 min observed evidence of a clean air shaft in the center of the cloud. This might be related to the apparent pure water plume observed for MILLRACE, even though details of the temporal behavior of the condensed water vapor cap differed considerably for DIAL PACK. (Green attributed the clear column to downward mixing of cool, clean air.) Specifically, DIAL PACK evidently produced a cap of condensed water vapor very early, as Green[6] notes that the cap started to evaporate at about T+3 to 5 min. In the case of MILLRACE, the condensed water cap was also valuable because of the opportunity it afforded us to scan both water and dirt plumes at essentially the same range. Unfortunately that range was rather long, as we were still confined to the holding pattern 18 km north of the debris cloud at this time.

T + 592 sec

Figure 12.   Photograph of the Explosion-Generated Water Cloud

D.   SCATTERING GEOMETRY

The sun-cloud-sensor geometry is illustrated in Figure 1. Solar radiation impinges on the top of a cloud layer at a zenith angle α. Scattered radiation is observed by the sensor which is positioned on a ray with zenith angle β. The angle between the azimuthal directions of the sun and the plane is defined to be γ. Then the scattering angle θ is defined by

$$\cos \theta = -(\cos \gamma)(\sin \alpha \sin \beta) - \cos \alpha \cos \beta$$

The probability that a photon of light will be scattered through a given angle θ is generally a function of particle size, composition and shape.

For fixed sun and sensor zenith angles, α and β, a limited range of scattering angles are possible. It can be shown that minimum θ is given by $180 - |\alpha + \beta|$ and maximum is given by $180 - |\alpha - \beta|$. For MILLRACE many of the cloud observations were made at sensor zenith angles near 90 deg and solar zenith angles around 38 deg. Approximate scattering angles were therefore in the range of 52 to 128 deg. Some observations of the late diffuse dust cloud were made at angles less than 50 deg and some observations throughout the test probably reached 180 deg.

IV. DISCUSSION OF THE OBSERVATIONS

A.   INFRARED OBSERVATIONS

An example of the data obtained on the dust/debris cloud is shown in Figure 13. The plot displays two successive spectra obtained with the higher sensitivity detector during a single 360 deg rotation of the CVF. Note that the scan begins at 1.8 μm, moves upward to 3.4 μm, and then returns to 1.8 μm. The spectra we obtained are all characterized by a rather strong peak near 2.15 μm, where the atmosphere is $\sim$90 percent transparent. Strong atmospheric absorptions at $\sim$1.9 μm (due to water vapor) and from 2.4 to 2.8 μm (due to H_2O and CO_2) sharply attenuate the flux from the clouds in
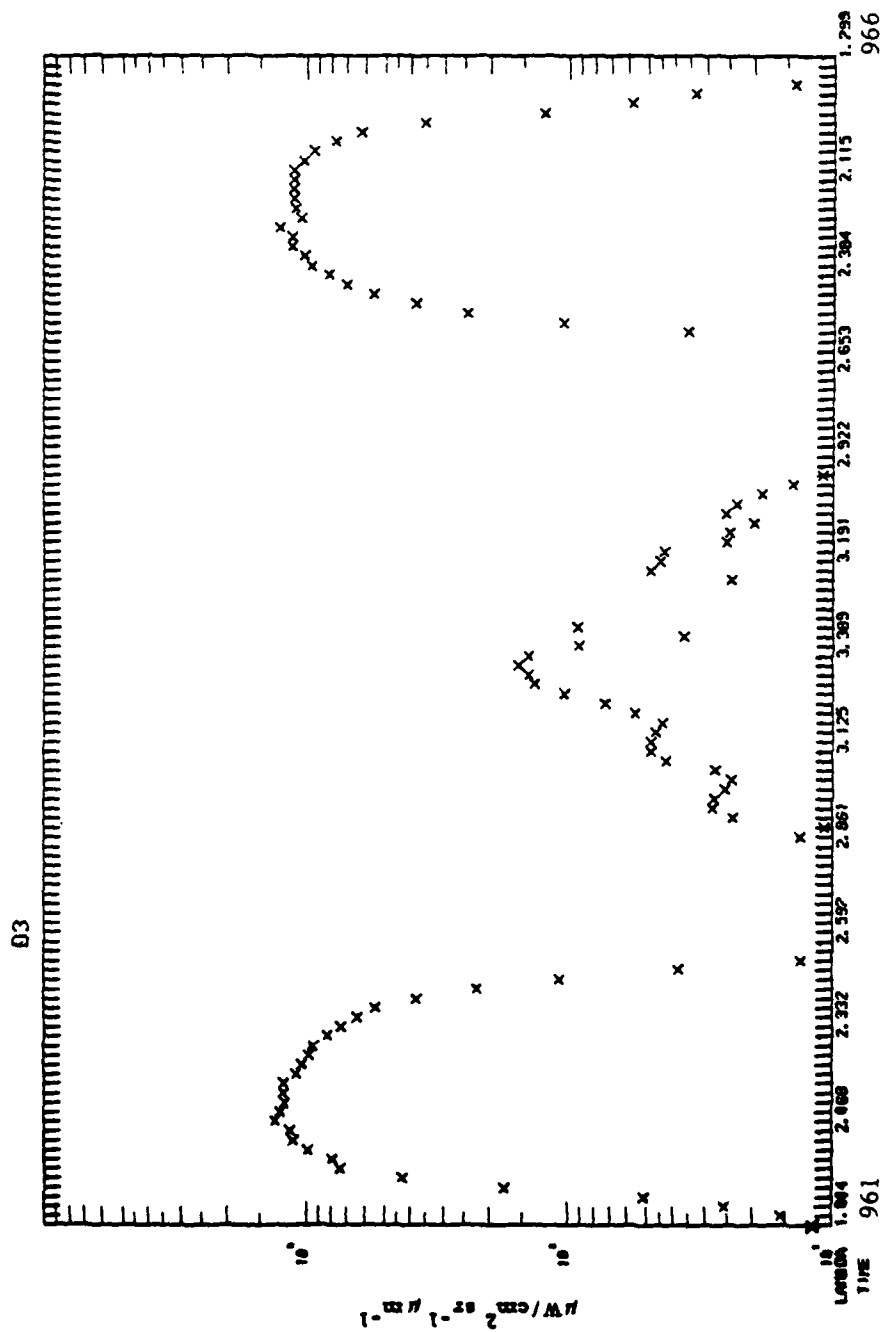
31

Figure 13. Dust Cloud Spectra

32

these regions. The spectra of the radiation scattered by water and dust clouds differ most in the 2.8 to 3.4 μm region, as can be seen by comparing the spectra in Figures 13 and 14. Figure 14 shows one of the spectral pairs (one rotation of the CVF) obtained at T+10 min with the spectrometer viewing on the water cloud which emerged above the dust cloud at about T+9 min (as discussed in Section III C). The dust cloud can scatter appreciably more flux than the water cloud in the 2.8 to 3.4-μm region, depending on particle size, relative humidity, and geometry.

The latter variable, geometry, was demonstrated to be particularly important during several circular maneuvers executed during our flight (see Section III A). After analyzing the data obtained on three of these maneuvers, the following pattern emerged. Each track began with a leg with an aircraft heading of ~300 deg, or a scattering angle of ~120 deg, during which time little or no 3-μm signal was detected from the dust cloud. Then, a relatively quick change to a more easterly heading with $\theta \lesssim$ 110 deg was made, and larger signals of varying strengths were detected at 2.8 to 3.4 μm. During one such maneuver at T+12 to T+15 minutes, we obtained 5 dual spectral scans with θ ~115 deg, and then 8 dual scans with θ ~ 90 deg. The average of the scans for these two ranges of scattering angles are shown in Figures 15 and 16. For this modest decrease in scattering angle ($\Delta \theta \approx 25^{\circ}$), the 2.15-$\mu$m flux increased by ~50 percent, while the 3-μm flux increased by about a factor of 5. (It is possible that part - perhaps a factor of ~1.5 - of the increase near 3 μm may be due to smaller absorption by water vapor along the line of sight to the cloud. The smaller absorption at ~1.9 μm in Figure 16 would tend to support this idea, but is is unlikely that the differences in 3-μm signal can be accounted for by this alone. Also, it would have to be more than coincidence to have the water vapor absorption decrease on three separate runs just as the plane's heading changed in this manner.)
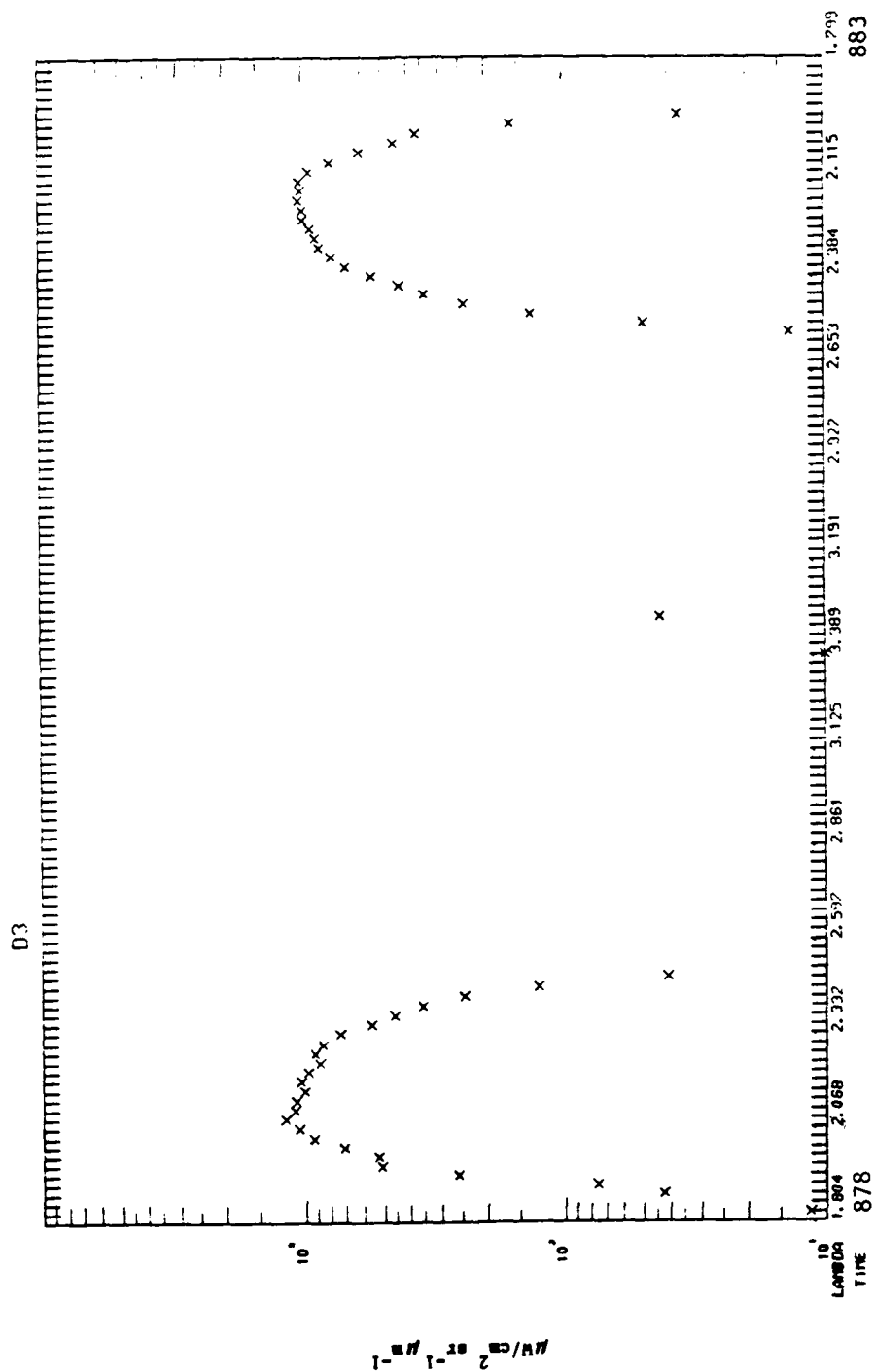
33

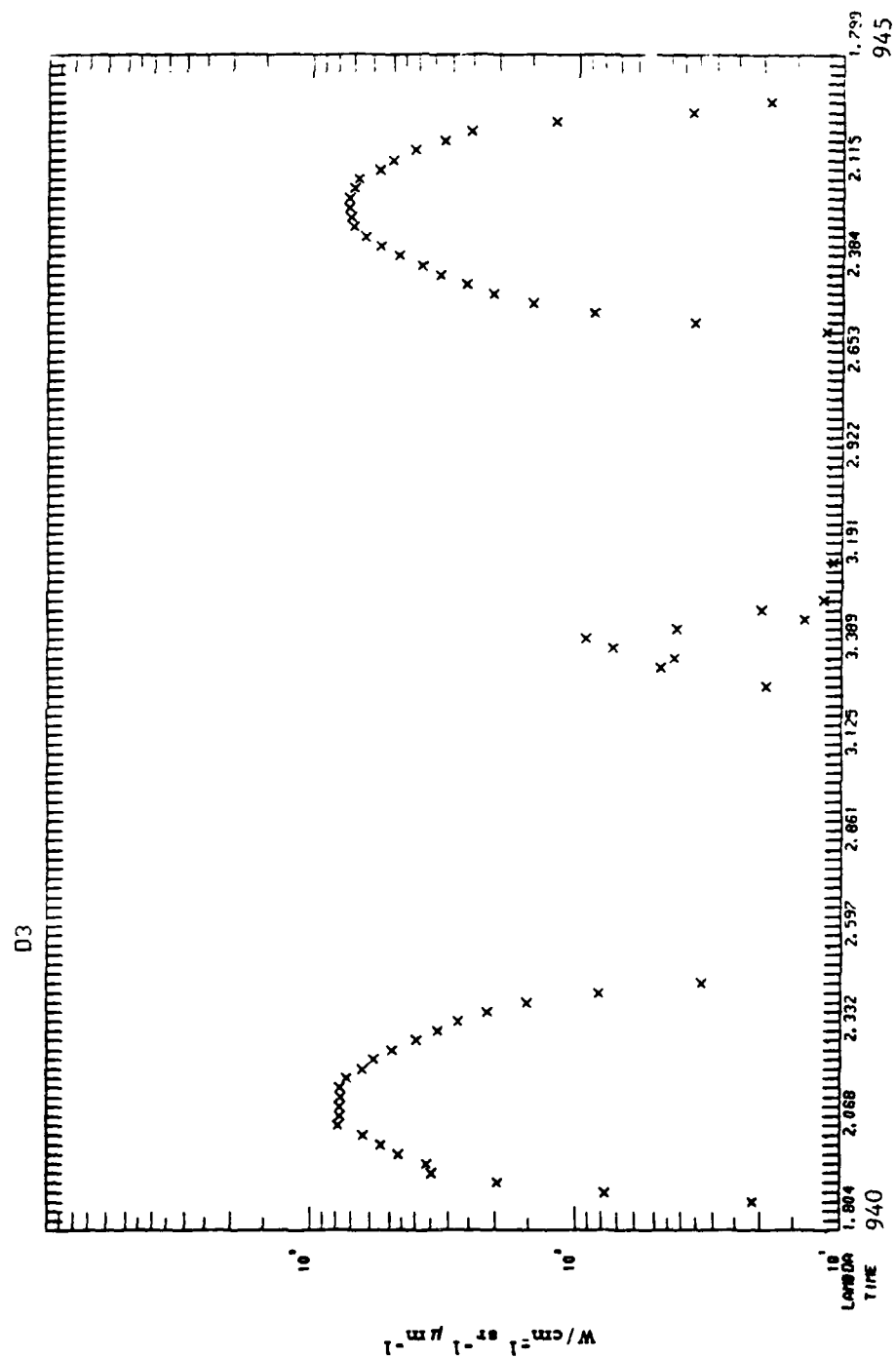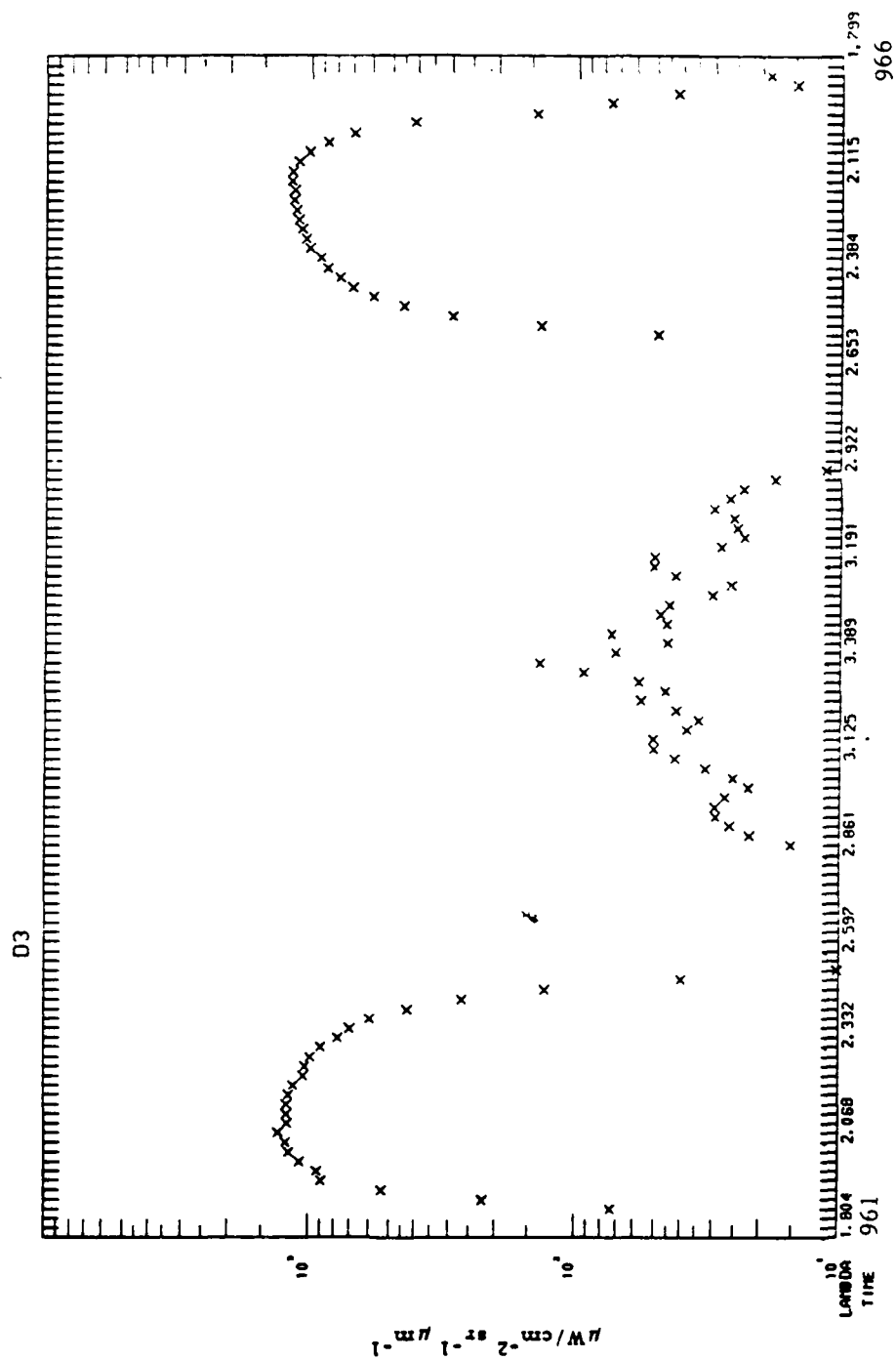Figure 14. Spectra of the Explosion-Generated Water Cloud

34

Figure 15. Dust Cloud Spectra with a Weak 3 μm Signal: θ Scattering = 115 degrees

35

Figure 16. Dust Cloud Spectra with a Strong 3 μm Signal: θ Scattering = 90 degrees

As noted above, these spectra (Figures 13 to 16) still exhibit the effects of absorption by the atmosphere along the path sun-cloud-observer. We have compared the positions of the flux peaks near 2.97 and 3.15 μm with peaks in the measured spectra of stars obtained in this wavelength from a ground-based observatory. The wavelengths of peak signal agree to within ~2/3 of a resolution element in spite of the difference in total water vapor absorption and instruments used for the two cases. Flight spectra at various times and scattering angles exhibit 2.97, 3.15 and 3.4-μm peaks. We attribute these spectral differences to the combined effects of atmospheric absorption along the line of sight to the cloud and varying amounts of flux scattered in the direction of our instrument.

Table 2 shows the ratio, R, of scattered flux at 2.15 μm to that at 3.15 μm for a variety of observing conditions. As we did not detect any significant 3-μm signal from the small water cloud above the dust cloud, even though it was observed at smaller scattering angles than the dust cloud, we empirically can only derive a lower limit on R for the water cloud. Thus, we proceeded to use a model for the scattering of infrared radiation by water clouds to derive the ratio expected for such a cloud under our observing conditions.

B.   IR SCATTERING FROM WATER CLOUDS

Previous measurements of IR scattering from water clouds as well as theoretical calculations indicated that the radiance near 3.0μm would be 1 percent or less of the 2.2-μm radiance. In the present instrument the 3.0-μm signal would be at or below measurement threshold when the 2.2-μm signal was in saturation. In order to provide an estimate of the 3.0-μm water cloud signal for comparison with the 3.0-μm dust cloud signal it was decided to utilize water cloud scattering codes which had been developed earlier by The Aerospace Corporation Chemistry and Physics Department.

Aerospace's Scattered Solar Radiance from Clouds, SSRC, code[8] models reflected solar radiation from a cloud as the solar reflectance from a uniform single layer plane-parallel, semi-infinite, cumulus cloud. The cloud may be composed of spherical water or ice particles. The scattering calculation is based on the Mie single-scattering model with an empirical correction for multiple scattering. The Aerospace code LOWTA 4, an enhanced version of the AFGL LOWTRAN 4 code, provides transmission factors for the sun-cloud-detector geometry. Transmission is especially reduced in the 2.5-2.9-μm band due to water vapor and is generally sensitive to atmospheric conditions. When it is run with radiosonde data from the MILLRACE test, LOWTA 4 provides input data to SSRC, from which scattering signatures unique to the test conditions can be derived.

C.   COMPARISON OF THEORY AND OBSERVATION

The resulting variation of radiance with wavelength and scattering angle (θ) is shown for a water cloud in Figures 17a to f. Inband radiance from 1.9 to 3.4μm was calculated using the code. It is seen that the radiance peaks at smaller θ, in agreement with our results on the dust cloud. However, the model predicts about the same effect at 2 μm (a factor of 1.8) compared to 3 μm (1.2) for scattering by a water cloud in direct contrast with the results presented here for a dust cloud where the 3-μm signal increases significantly faster at smaller θ than the 2.15-μm signal. The variation of radiance with scattering angle measured at 2.7 μm by previous experiments (data from Ref. 2) with water clouds is shown in Figure 18. Again, the signal is strongly peaked about θ = 0 deg.

Figure 17a. Theoretical Water Cloud Spectra A, B, C = 4.27, 4.42, 4.57, km Clouds, D = Surface
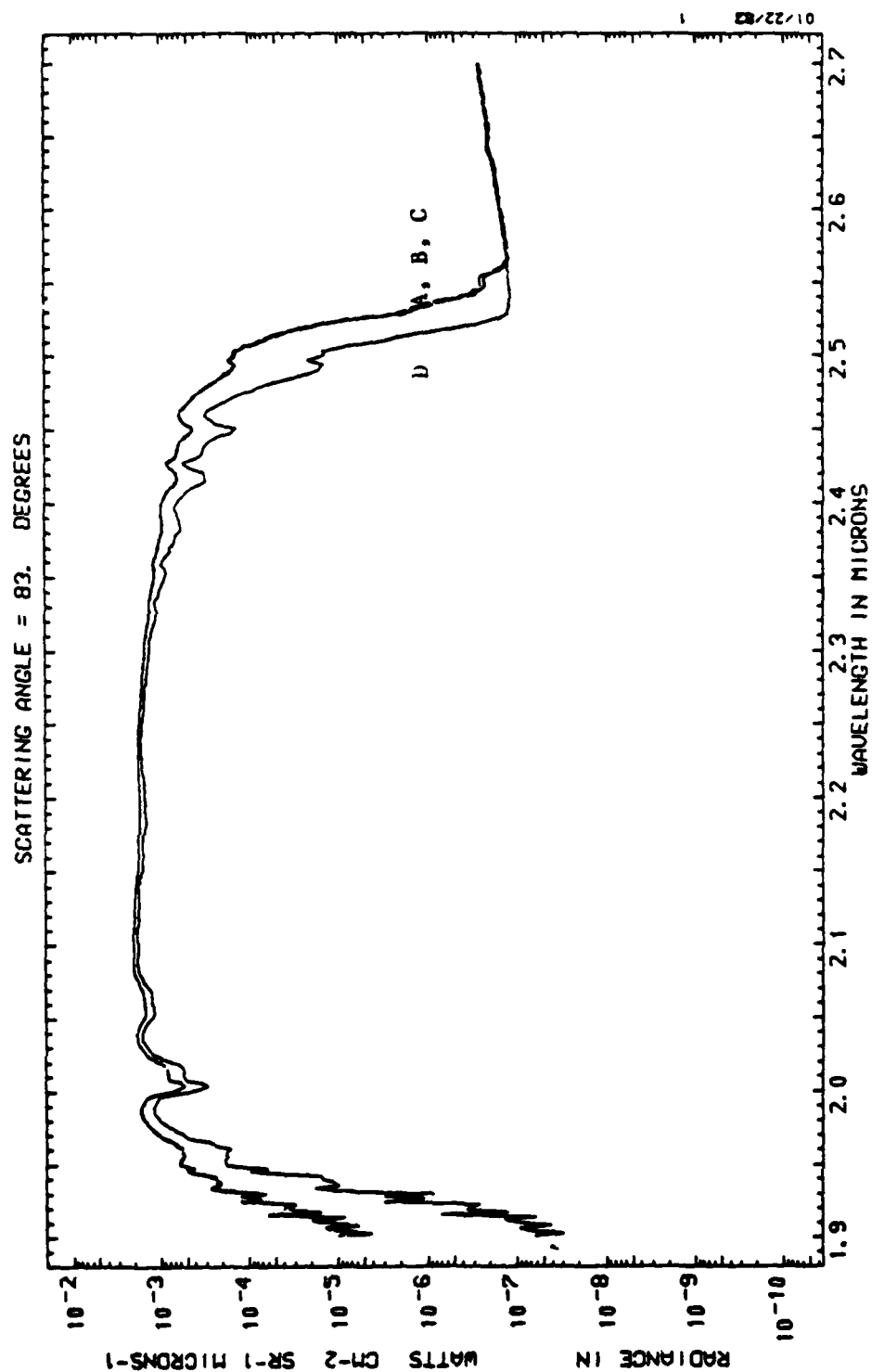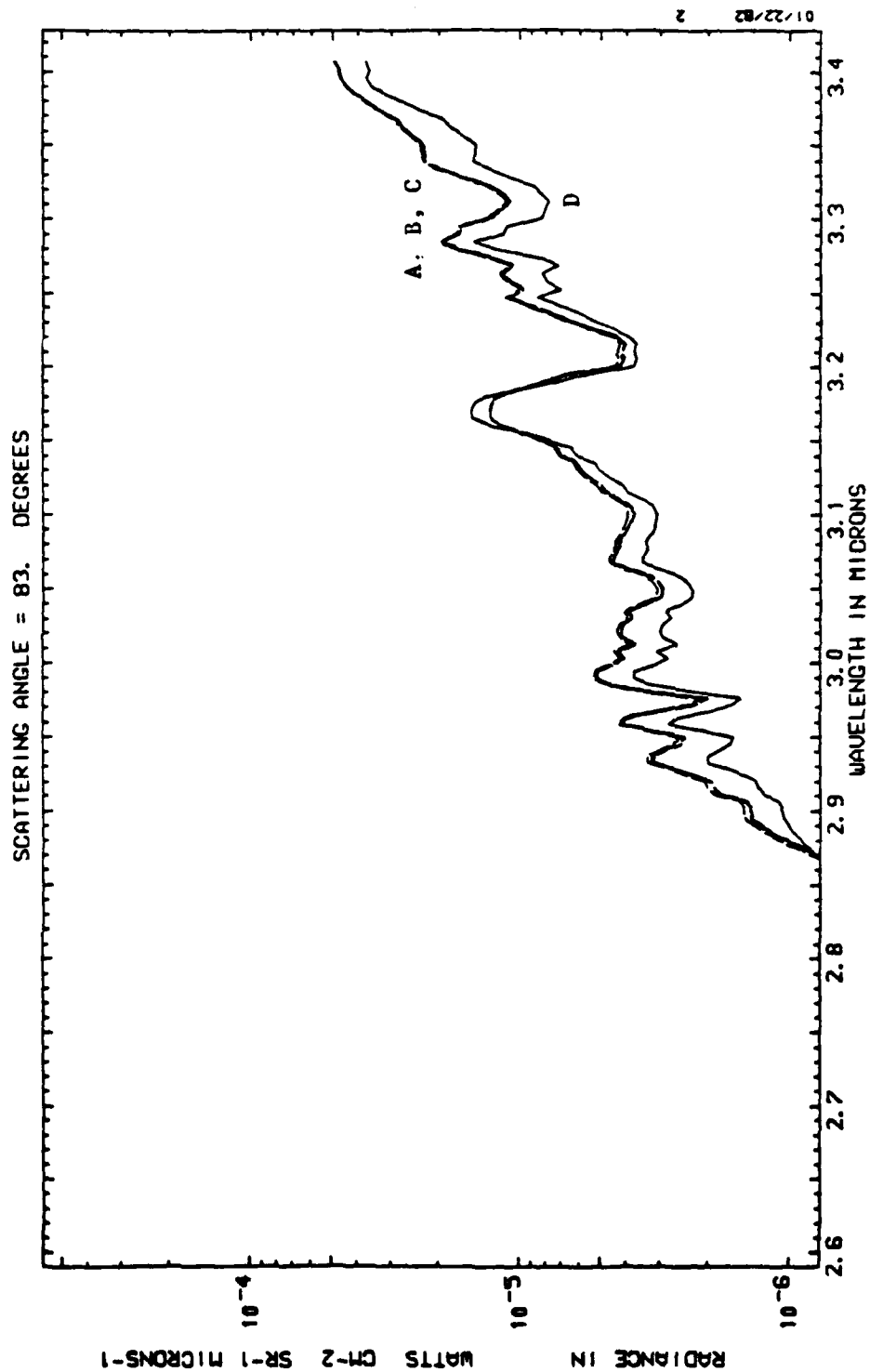
39

Figure 17b. Theoretical Water Cloud Spectra A, B, C = 4.27, 4.42, 4.57, km Clouds, D = Surface

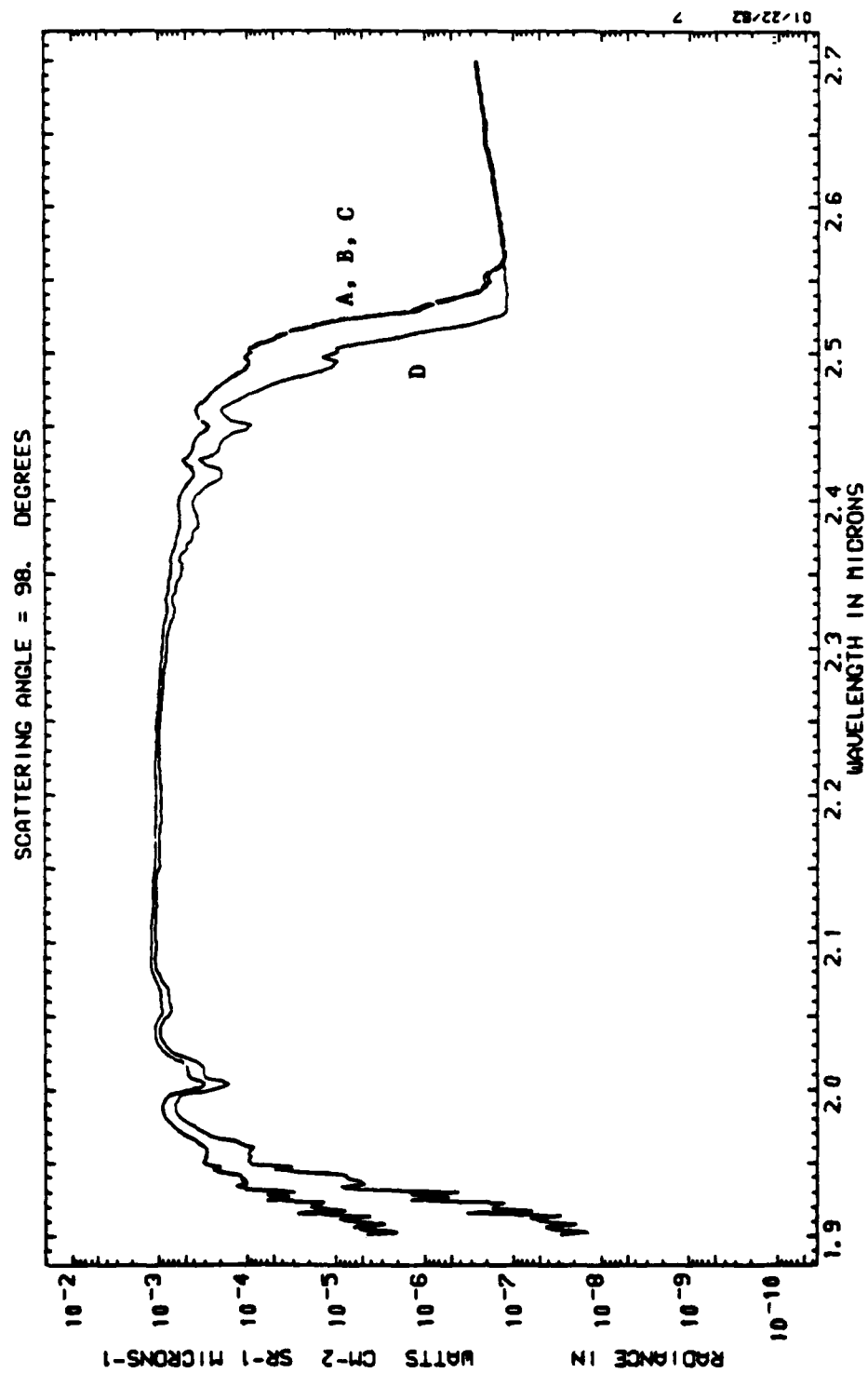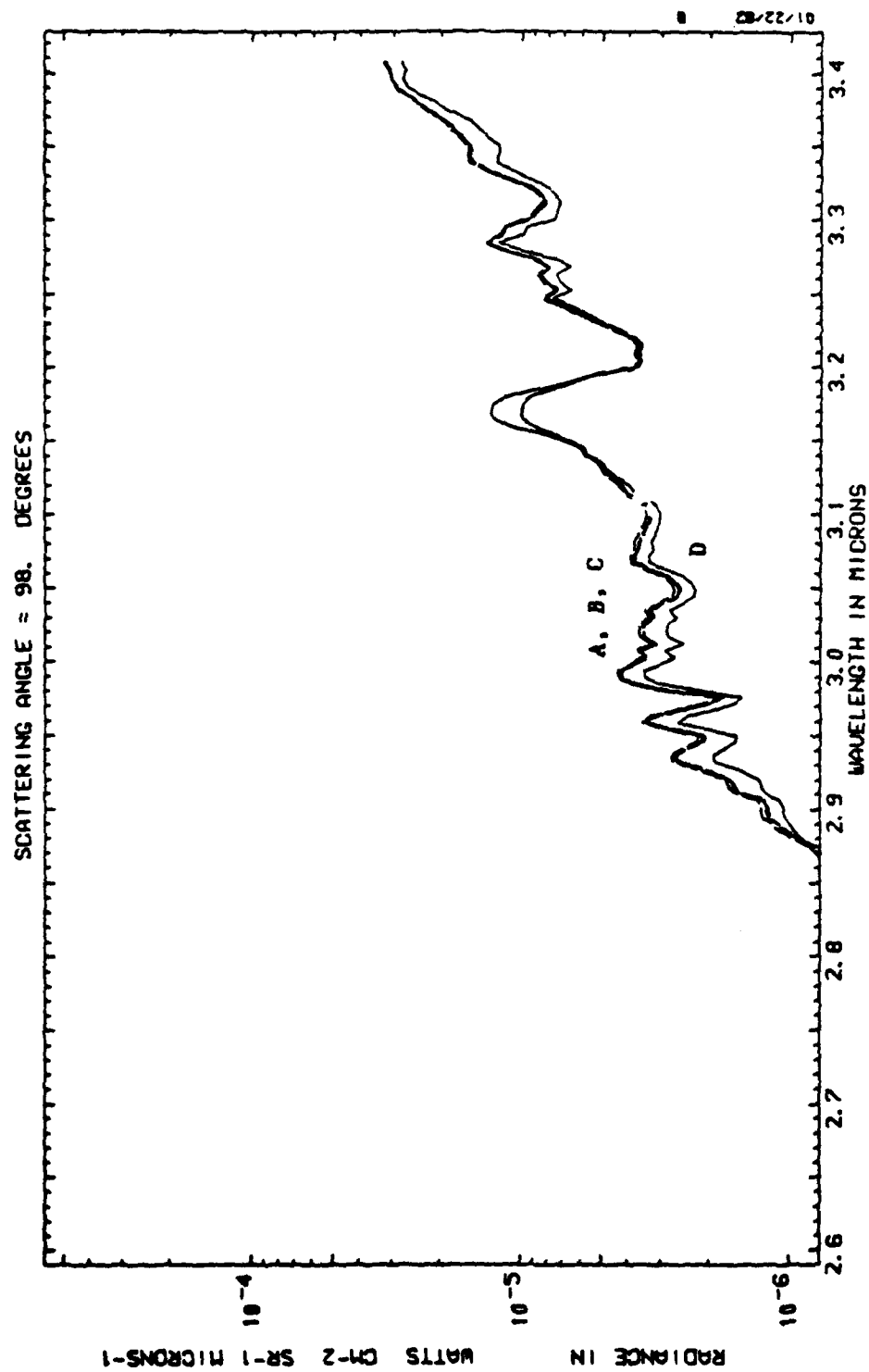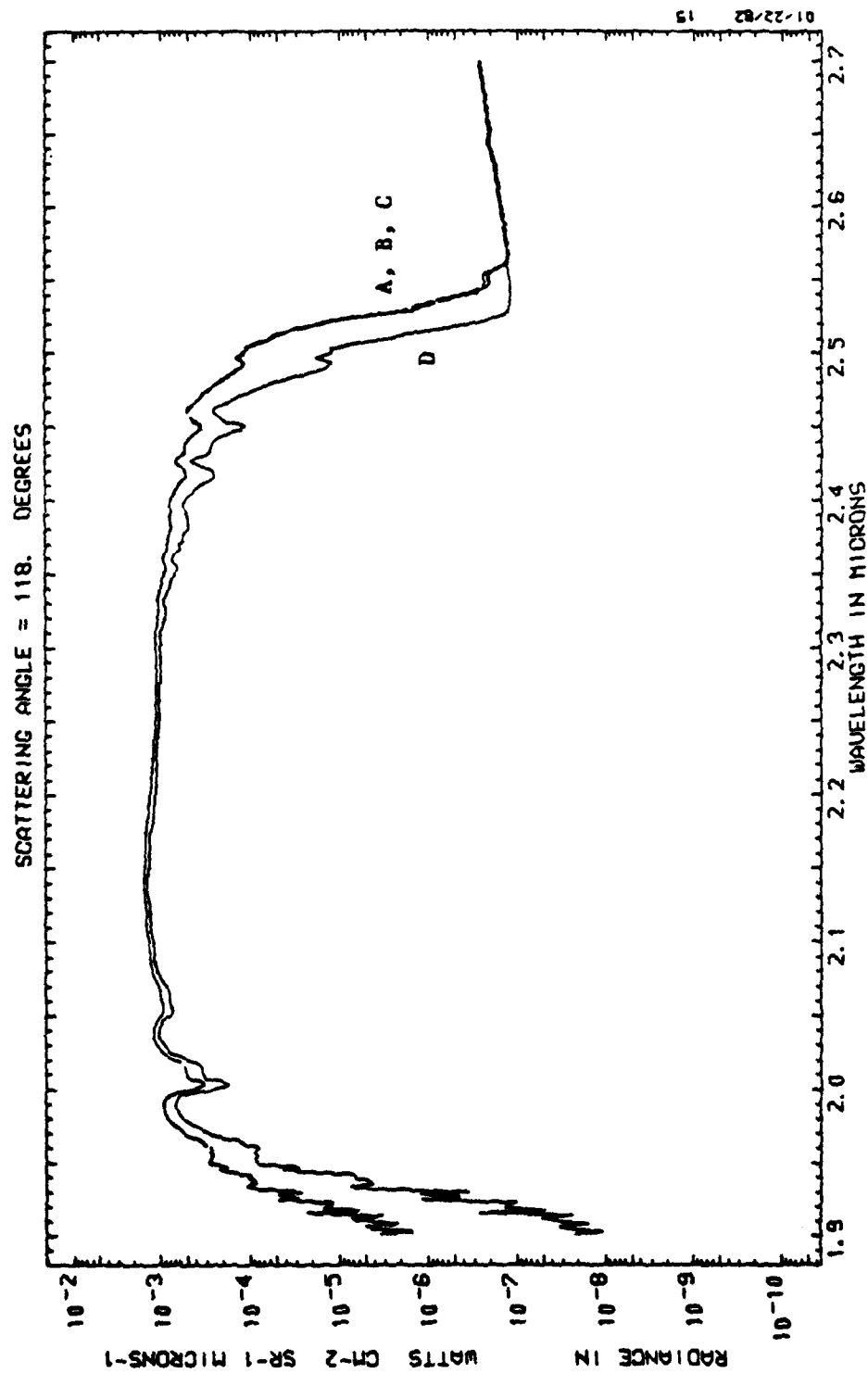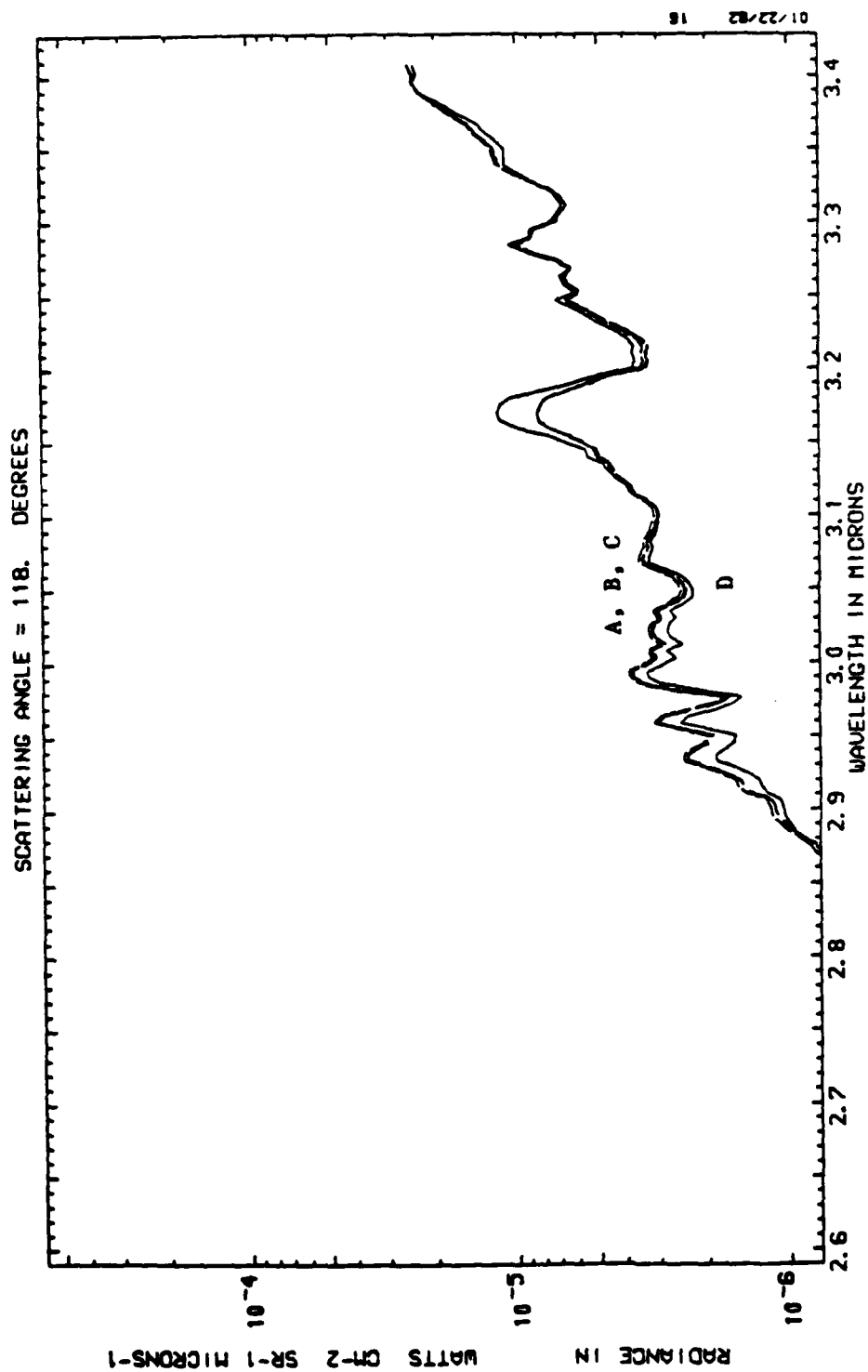Figure 17c. Theoretical Water Cloud Spectra A, B, C = 4.27, 4.42, 4.57, km Clouds, D = Surface
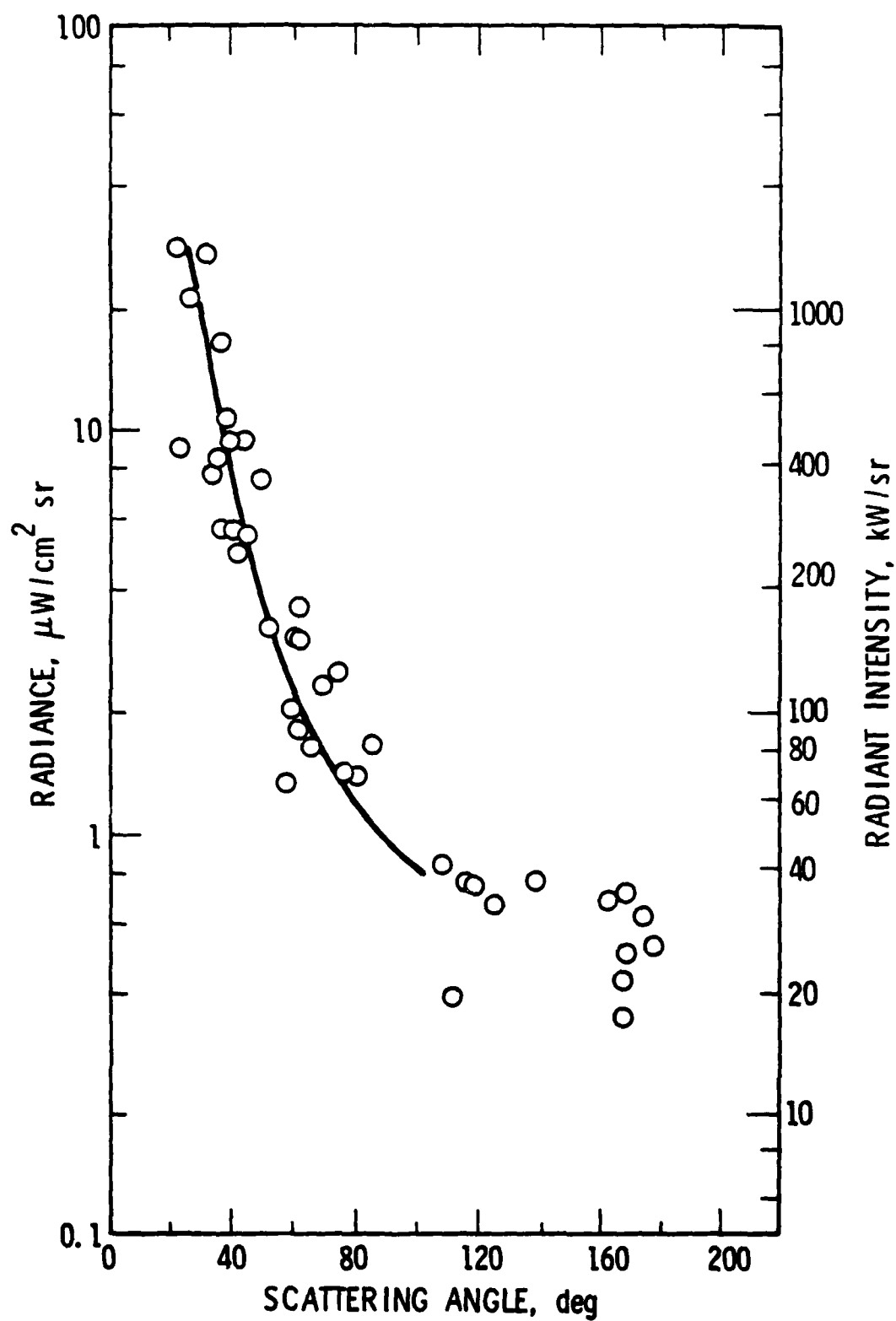
41

Figure 17d. Theoretical Water Cloud Spectra A, B, C = 4.27, 4.42, 4.57, km Clouds, D = Surface

42

Figure 17e. Theoretical Water Cloud Spectra A, B, C = 4.27, 4.42, 4.57, km Clouds, D = Surface

43

Figure 17f. Theoretical Water Cloud Spectra A, B, C = 4.27, 4.42, 4.57,
km Clouds, D = Surface

44

Figure 18. Measured Water Cloud Radiance at 2.7 μm versus Scattering Angle

TABLE 2. Ratio of Scattered Flux at 2.15 μm to 3.15 μm and to 3.4 μm for

Different Scattering Angles

Time (minutes after blast)	$I_{2.15}/I_{3.15}$	$I_{2.15}/I_{3.3-3.4}$	scat. (deg)
Dust Clouds			
11.4 - 11.9	78	13	117
12.0 - 12.7	24	12	109
15.0 - 15.9	37	13	158
15.9 - 16.7	17	12	86
54.3 - 54.7	29	18	68
54.7 - 55.7	35	15	56
Water Clouds			
9.7 - 10.0	300	30	98
58.8 - 59.1	100	220	127
59.2 - 59.7	200	200	130

Note: We estimate the error in these ratios to be less than 40 percent.

Calculated radiances as shown in Figure 17 can be used to scale the observed 2.15- μm signal on the water cloud to obtain an estimate of the expected signal in the 2.8 to 3.4- μm region. This estimate is below the level of detectability with our present instrument and is thus consistent with our data on the water cloud. We can now use the model value of R for the water cloud (~200 to ~100 depending on what λ is chosen) to compare with the observed values of R on the dust cloud (~40 to ~10). There is thus about a factor of 5 to 10 difference in the ratio, R, between the dust and water clouds.

V. CONCLUSIONS

MILLRACE proved to be an excellent laboratory for performing IR measurements. In contrast to our earlier measurements of artificial dust clouds where cloud persistence and limited scattering angles proved troublesome, MILLRACE provided a high density, long persistence cloud of sufficient size to facilitate measurements over a variety of scattering angles and altitudes. The explosion-generated water cap along with natural water clouds in the vicinity provided valuable supplemental data. From the aircraft platform measurements could be obtained at sufficient altitude to reduce water and CO_2 absorption effects.

Interchange of data among ground support and the experimenters provided valuable information not available in our earlier measurements. The ground control radar track was used in the calculation of scattering angles. Radiosonde data from one experiment were incorporated in the atmospheric model for the LOWTA transmission and SSRC codes. Ground-based photographs of the dust cloud were obtained from another experimenter and were used to estimate cloud height and width.

Measured water cloud radiances near 2.15 μm and radiances obtained from the Aerospace water cloud scattering model are in excellent agreement, providing experimental verification of the model as well as confirming our measurement technique. As was suggested by earlier experiments, we measured a 5 to 10 times larger radiance in the 3 to 3.4-μm band for a dust cloud compared to that of a water cloud. The difference in radiance between the two types of cloud is a function of cloud height, observer to cloud distance, atmospheric moisture content and the measurement scattering angle.

Experience gained from our measurements suggests improvements in instrumentation, notably the choice of detectors and electronic design, that

would increase system performance – especially in the 2.9 to 3.5-μm band. The increased sensitivity would allow a determination of water and dust cloud radiances over a wider range of experimental conditions in future tests.
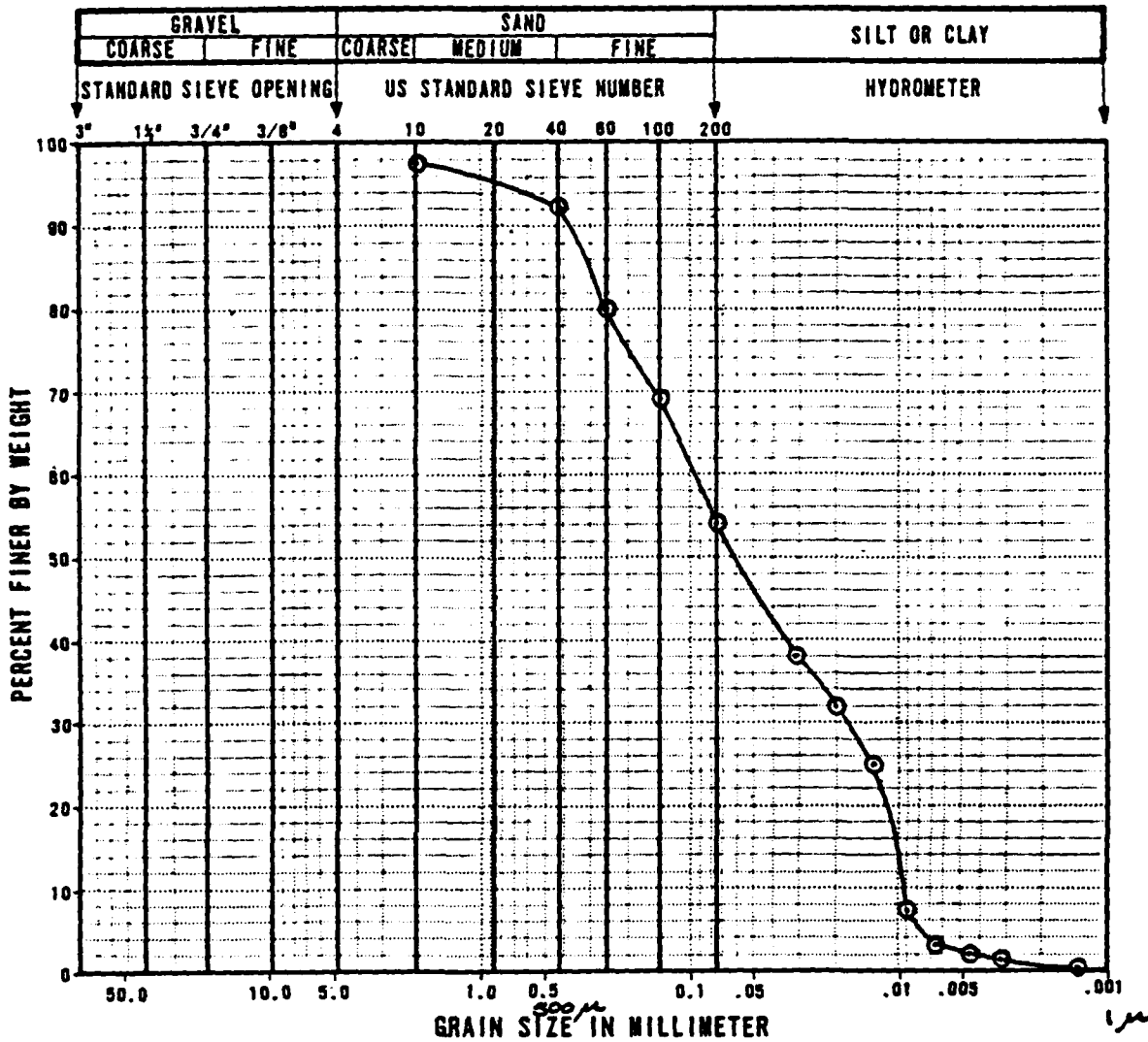
ACKNOWLEDGMENTS

REFERENCES

1.   Reid, G. H., LCDR USN, "MILLRACE Program Document," POR 7071, DNA, Kirtland Air Force Base, November 1980.

2.   Blau, H. H., et al., "Infrared Spectral Properties of High Altitude Clouds," TR 2, Arthur D. Little, Inc., December 1963.

3.   Burns, A. A. and Crawley, P. L., "Dice Throw UHF/SHF Transmission Experiment," Vol. III, DNA 4216T-3, SRI International, August 1979.

4.   Gould, Kenneth, "High-Explosive Field Tests: Explosion Phenomena and Environment Impacts," DNA KT-81-004, DASIAC, to be released.

5.   Reed, Jack, "MILLRACE-off-site Blast Predictions and Measurements," MILLRACE Results Symposium March 16-18, 1982, to be published.

6.   Green, W. D., "Airborne Sampling and Analysis of Particulates from the Dial Pack Event," DASA 2600, Defense Atomic Support Agency, January 1971.

7.   Thomas, C. R. and Cockayne, J. E., "Misers Bluff II Cloud Sampling Program: Data Summary and Dust Cloud Characterizations," DNA 5189F, Science Applications, Inc., December 1979.

8.   Young, S. J., "Scattering of Solar Radiation by Clouds," SAMSO-TR-78-178, Aerospace Corp., December 1978.

9.   Knollenberg, R. G., "Results of the Misers Bluff II Aircraft Dust Particle Sampling Experiments," DNA 4951F, Particle Measuring Systems Inc., May 1979.

10.   Ashley, G. W., et al., "Background Spectral Radiance and Contrast in the Near U.V., Mid IR, LWIR Region," TM-6-125 PH-438, General Dynamics, March 1976.

APPENDIX

Test Site Soil - Size Analysis

	GRAVEL		SAND			SILT OR CLAY
	COARSE	FINE	COARSE	MEDIUM	FINE	
STANDARD SIEVE OPENING			US STANDARD SIEVE NUMBER			HYDROMETER

GRAIN SIZE DISTRIBUTION

SYMBOL	BORING NUMBER	SAMPLE NUMBER	SAMPLE DEPTH (FEET)	SOIL TYPE
————	DESERT SOIL			
— — —				
—·——·——				

The percentage of particles finer than 500 micron (µ) by weight is

93 percent. The specific gravity of the soil is 2.68.

≣Ertec
The Earth Technology Corporation

GRAIN SIZE DISTRIBUTION

LABORATORY OPERATIONS

The Laboratory Operations of The Aerospace Corporation is conducting experimental and theoretical investigations necessary for the evaluation and application of scientific advances to new military space systems. Versatility and flexibility have been developed to a high degree by the laboratory personnel in dealing with the many problems encountered in the nation's rapidly developing space systems. Expertise in the latest scientific developments is vital to the accomplishment of tasks related to these problems. The laboratories that contribute to this research are:

Aerophysics Laboratory: Launch vehicle and reentry aerodynamics and heat transfer, propulsion chemistry and fluid mechanics, structural mechanics, flight dynamics; high-temperature thermomechanics, gas kinetics and radiation; research in environmental chemistry and contamination; cw and pulsed chemical laser development including chemical kinetics, spectroscopy, optical resonators and beam pointing, atmospheric propagation, laser effects and countermeasures.

Chemistry and Physics Laboratory: Atmospheric chemical reactions, atmospheric optics, light scattering, state-specific chemical reactions and radiation transport in rocket plumes, applied laser spectroscopy, laser chemistry, battery electrochemistry, space vacuum and radiation effects on materials, lubrication and surface phenomena, thermionic emission, photosensitive materials and detectors, atomic frequency standards, and bioenvironmental research and monitoring.

Electronics Research Laboratory: Microelectronics, GaAs low-noise and power devices, semiconductor lasers, electromagnetic and optical propagation phenomena, quantum electronics, laser communications, lidar, and electro-optics; communication sciences, applied electronics, semiconductor crystal and device physics, radiometric imaging; millimeter-wave and microwave technology.

Information Sciences Research Office: Program verification, program translation, performance-sensitive system design, distributed architectures for spaceborne computers, fault-tolerant computer systems, artificial intelligence, and microelectronics applications.

Materials Sciences Laboratory: Development of new materials: metal matrix composites, polymers, and new forms of carbon; component failure analysis and reliability; fracture mechanics and stress corrosion; evaluation of materials in space environment; materials performance in space transportation systems; analysis of systems vulnerability and survivability in enemy-induced environments.

Space Sciences Laboratory: Atmospheric and ionospheric physics, radiation from the atmosphere, density and composition of the upper atmosphere, aurorae and airglow; magnetospheric physics, cosmic rays, generation and propagation of plasma waves in the magnetosphere; solar physics, infrared astronomy; the effects of nuclear explosions, magnetic storms, and solar activity on the earth's atmosphere, ionosphere, and magnetosphere; the effects of optical, electromagnetic, and particulate radiations in space on space systems.